CHRONOSTRATIGRAPHIC DATABASE FOR UPPER CRETACEOUS OCEANIC RED BEDS (CORBs)

ROBERT W. SCOTT
Precision Stratigraphy Associates and University of Tulsa, RR3 Box 103-3, Cleveland, Oklahoma 74020, U.S.A.
e-mail: rwscott@ix.netcom.com

Abstract: An integrated, testable chronostratigraphic database of Late Cretaceous bioevents in numerous reference sections was constructed in order to test the global synchrony of Upper Cretaceous oceanic redbeds—CORBs—and to measure precisely their rates of sediment accumulation. Graphic correlation was the method of choice because it is based on species checklists and because the range projections are transparent and testable. Stage boundaries are defined by GSSP or key reference sections with ammonites, planktic foraminifera, and nannofossils, as well as with magnetochrons. Sequence boundaries and other sedimentary markers as defined in reference sections are projected into the database by graphic correlation of the co-occurring fossils. The database scale is calibrated to radiometric ages of Upper Cretaceous stages that are generally similar to those of the 2004 time scale.

This database is used in three areas to interpret deposition of CORBs, the North Atlantic, the Swiss Pre-Alps, and the Eastern Austrian Alps. North Atlantic CORB intervals in six cores range in age from Turonian to Maastrichtian. This succession was deposited within two distinct deep water masses. A Turonian–Santonian oxygenated water mass with a relatively shallow calcite compensation depth (CCD) hosted red-bed deposition and diversification of benthic foraminifera. Deep-water, low pH conditions existed in the North Atlantic during Late Cretaceous submarine volcanism. The well oxygenated Campanian–Maastrichtian water mass was above the CCD, and calcareous fossils were preserved during a second benthic foraminifer diversification event. Red marine clay and turbidites alternated with gray and green beds. Rates of sediment accumulation generally were higher during the Campanian–Maastrichtian period than during the earlier period.

CORB strata in the Swiss Pre-Alps were deposited at different times in different places for varying durations and at different rates beginning in the Aptian and continued sporadically into the Santonian. In the Eastern Alps Upper Cretaceous marine red beds are interbedded with siliciclastic and calcareous facies deposited in the Penninic Ocean between colliding plates. Oldest CORB deposition is recorded in the Albian and became persistent during the Campanian. Interbedded red and gray strata record climatic forcing during tectonically controlled transgressive events.

The duration of CORB deposition generally was shorter in epicontinental basins than in oceanic basins, but the average rate of sediment accumulation tended to be similar in epicontinental and oceanic basins. Even-bedded CORBs were deposited at the same average duration as homogeneously bedded deposits, but even-bedded CORBs accumulated faster than homogeneous deposits. Many repetitively interbedded oceanic red beds were deposited at rates close to orbital frequencies and may have been related to climatic forcing.

Keywords: Upper Cretaceous chronostratigraphy, nannofossils, planktic foraminfera, benthic foraminifera, CORB accumulation rates, CORB durations

INTRODUCTION

Upper Cretaceous oceanic red beds are widespread in the Tethys and locally at higher latitudes and were preceded by Lower Cretaceous red deposits (Hu et al., 2005a; Hu et al., 2005b; Wang et al., this volume). Two initial goals of the IGCP 463 project were (1) the timing of deposition of these strata in different basins and (2) the number of deep oceanographic oxic events. Detailed biostratigraphic studies of numerous Upper Cretaceous CORB sections have shown that they are of different ages in different basins, ranging from Early Turonian to Late Maastrichtian. In some basins CORB deposition recurred multiple times. To achieve these goals, a global biostratigraphic database was constructed by integrating the first and last appearances of major fossil taxa with radiometrically dated beds, chemostratigraphic events, and magnetochrons. A quantitative methodology was used in order to objectively integrate Upper Cretaceous stage boundaries of the 2004 time scale (Ogg et al., 2004) and to interpolate ages into the various sections of the CORB project by a testable method. Using the 2004 time scale as a time framework, this study interpolates the ages of chronostratigraphic events, such as bioevents and chemostratigraphic events, by their spacing in numerous sections relative to the numerical ages of proven marker horizons. The ages of most stages are within the error range of the ages in the 2004 scale.

CORBs—Cretaceous oceanic red beds—were deposited intermittently beginning at least during Late Aptian to the end of Maastrichtian times and even into the Paleogene (Hu et al., 2005a; Hu et al., 2005b). During the Late Cretaceous, CORBs were deposited in deep epicontinental basins that formed on continental crust between colliding continents or on the craton. Examples come from Spain, northwestern Germany (Fenner, 2001; Wiese, this volume), Austria, Poland, the Czech Republic, Romania, the Caucasus, and Tibet. CORBs were also deposited on oceanic crust in the Atlantic and eastern Pacific basins. Some CORBs have homogeneous bedding without distinct sedimentary structures and no carbonate, and others are regularly and repetitively evenly bedded with nannofossil marl and limestone.

Three widespread anoxic events separate CORBs: the Aptian OAE 1a, the Late Cenomanian OAE 2, and the more local Santonian OAE 3. Aptian to Cenomanian CORBs are calcareous, pelagic oozes with nannofossils and planktic foraminifera deposited on the outer shelf to slope in water depths up to 500 m. Turonian to Maastrichtian CORBs are shallow to deep epicontinental and

Cretaceous Oceanic Red Beds: Stratigraphy, Composition, Origins, and Paleoceanographic and Paleoclimatic Significance
SEPM Special Publication No. 91, Copyright © 2009
SEPM (Society for Sedimentary Geology), ISBN 978-1-56576-135-3, p. 35–57.

oceanic abyssal deposits, some of which are homogeneous and some are cyclically bedded.

GLOBAL BIOSTRATIGRAPHIC DATABASE

In the past two decades a number of published Cretaceous biostratigraphic range charts show the stratigraphic order of fossils based on the collective interpretations of specialists (Bralower et al., 1995; Hardenbol and Robaszynski, 1998; Burnett, 1998; Premoli Silva and Sliter, 2002; Ogg et al., 2004). These range charts present the first and last occurrences (FOs, LOs) of numerous age-diagnostic ammonites, foraminifera, nannofossils, and dinoflagellates, among other groups. Some of these charts integrate bioevents with radiometric ages and with magnetochrons and interpolate numerical ages to the bioevents. Because these charts represent the most current understanding of fossil ranges by various biostratigraphic specialists, they serve as the point of comparison for subsequent databases. However, these compilations do not document the actual sections studied or the check-list data matrix, from which the range charts were derived. Nor do these charts clearly show the methods of interpolation of numeric ages derived from radiometry.

Graphic correlation is one of several quantitative stratigraphic methods that objectively integrate data from measured sections in such a way that the data sources are identified and verified, and the interpolations tested. Biostratigraphic databases are the result of thousands of paleontologic observations, and their integration must be scientifically testable. Quantitative stratigraphic methods make such testing and evaluation possible. To this end the MIDK42CS.2 Cretaceous Chronostratigraphic Database was constructed by means of graphic correlation using the software GraphCor© (Hood, 1995). This database integrates the ranges of nearly 3000 taxa of planktic and benthic foraminifera, nannofossils, dinoflagellates, ammonites, inoceramids, magnetochrons, radiometric dates, geochemical events, and selected sequence stratigraphic markers defined in published reference sections. Stage boundaries as defined by Ogg et al. (2004) were integrated into this database and calibrated to the new age scale except for two cases, the base of the Cenomanian and the base of the Maastrichtian, which will be discussed further.

Data Sources

The MIDK42CS.2 Chronostratigraphic Database was compiled for the CORB Cretaceous time scale from published reports of 150 outcrops and cored sections globally distributed (Appendix 1). These reports give the location and geologic setting of each section. They also present the ranges or even the actual specimen numbers per sample in a measured section or core. The additional CORB localities are mainly in the Tethyan realm and range from China to North Atlantic (see Figure 1 in Wang et al., this volume). Section files were prepared for each locality, consisting of the first and last stratigraphic positions of species in meters or feet of the measured section or cored interval. The references and authorships of the taxonomic identifications are noted. Two types of data comprise section files: (1) rows for each species, its morphologic group, and its base and top in meters or feet, and (2) comment lines preceded by an asterisk (*), which means that this information is not utilized by GraphCor. Two other sections are actually composites of sets of sections. The WOODCS.1 section is a composite of four Turonian–Coniacian sections in northwestern Germany, including the Salzgitter–Salder Quarry (Wood et al., 1984). The PECOSCS.1 section is composed of Albian–Cenomanian carbonate outcrops along the Pecos River in Texas, U.S.A. (Scott and Kerans, 2004).

Process of Data Integration

Graphic correlation is a quantitative, non-statistical technique that determines the coeval relationships between two sections by comparing the ranges of event records in both sections (Shaw, 1964; Carney and Pierce, 1995). A graph of any pair of sections is an *X*-*Y* plot of the FOs (bases) and LOs (tops) of taxa found in both sections. The interpreter places a line of correlation (LOC) through the tops and bases that are at their maximum range in both sections. This LOC is the most constrained hypothesis of synchrony between the two sections and alters the fewest bioevents. The LOC also accounts for hiatuses or faults at stratal discontinuities indicated by the lithostratigraphic record. The position of the LOC is defined by the equation for a regression line. Explanation and examples of the graphic technique are illustrated by Miller (1977) and Carney and Pierce (1995).

This original method of graphic correlation compares the spacing of events in terms of thickness of the SRS (Shaw, 1964; Carney and Pierce, 1995; Gradstein et al., 2004a). A new method is to graph the SRS to a time scale so that the events are directly projected into numerical ages. The MIDK3 database was constructed in this way by graphing the Cenomanian–Turonian section at Kalaat Senan, Tunisia, to the 1989 time scale (Harland et al., 1990; Scott et al., 2000). The sedimentology, sequence stratigraphy, and biostratigraphy of this section were carefully documented and the section recorded continuous deposition at a uniform rate (Robaszynski et al., 1990; Robaszynski et al., 1993). The stage boundaries were clearly and unequivocally defined biostratigraphically so that the LOC could be pinned to them. Thus all events were related to time. To further constrain the numeric ages of the database scale, sections with numerically dated beds were graphed and the *X*-axis scale was recalibrated to millions of years (megaannum, Ma) (Carney and Pierce, 1995; Scott et al., 2000).

The *X*-*Y* plot compares the rate of sediment accumulation (RSA) in one section with that in the other (Miller, 1977). The RSA does not account for compaction or other processes that reduce the thickness of the interval from its initial depositional thickness; thus, the sedimentation rate is not measured. The technique of graphic correlation enables the stratigrapher to consider sedimentologic events together with the biotic events and test conclusions based on sedimentology with those based on fossils. Also, the event beds may add to the precision and accuracy of the correlation.

The new method of graphic correlation produces a comprehensive database that avoids the limitations of the method noted by Gradstein et al. (2004a). The ranges of more than 2000 bioevents and other markers are calculated instantaneously and used in the interpretation of each subsequent section. If the analyst prefers to use average ranges, GraphCor has the capability to average the ranges, which are the data points used in ranking and scaling (RASC) (Gradstein et al., 2004a). Also like the RASC method, graphic correlation plots all data points common to both the *X* and *Y* sections. Unlike RASC, graphic correlation plots the maximum or average position of the data points on the *X* axis.

Catalog Files. These files are lists of the sections that are graphed to build the range data. Normally each catalog file is limited to 50–60 sections because GraphCor recalculates the positions of bioevents each time a catalog of sections is opened. Each list is a "project", and the range data in all sections of a project are saved in a composited standard file that lists the species and their range end points. Successive projects incorporate additional sections, and the composited ranges become the SRS of the next project. The CORB database is the compilation of 150 sections in four projects that were compiled in order from MIDK3, MIDK4, MIDK41, to MIDK42 (Fig. 1; Appendix 1). So the

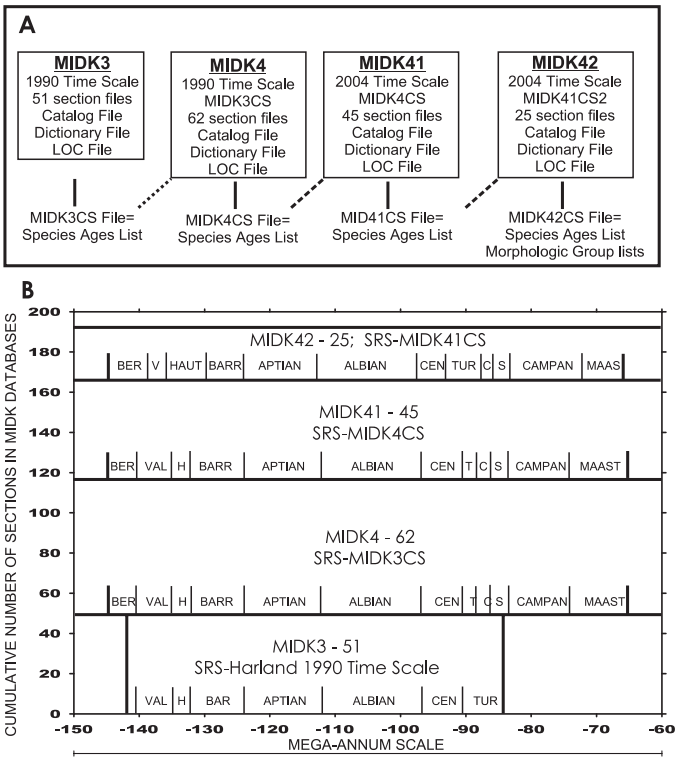

FIG. 1.—Diagram showing evolution of calibrating project MIDK42CS to time. **A)** Four steps in graphing 188 sections to compile the ranges of more than 2000 taxa and converting from the 1990 to the 2004 time scales. **B)** Comparison of the time scale used in the various projects from bottom to top, showing the cumulative number of sections in successive projects. The number of sections in each project is indicated after the project name; SRS is standard reference section to which all subsequent sections were graphed. This chart shows how the ages of the stage boundaries changed in the more developed databases.

database MIDK42CS.2 integrates ranges from all sections in these four projects. The time scales of each project have been adjusted to accommodate new radiometric data.

Dictionary Files.—

The taxa of all sections in each project are saved in a dictionary as DCT files. These files are lists of species and other chronostratigraphic markers such as magnetochrons and geochemical marker beds (OAE 2). The types of markers are grouped into geologic categories, such as nannofossils and sedimentary marker beds, and are sorted by their morphologic codes. Morphologic codes enable the different taxonomic groups to be sorted and inspected by specialists. GraphCor builds these files from the section files. "Look-up" tables of nannofossils (NN), planktic foraminifera (FP), benthic foraminifera (FB), dinoflagellates (DN), ammonites, (AM), magnetochrons (MA), marker beds (MB), and geochemical events (GC) for the CORB project are presented in appendices.

Line of Correlation Files.—

These files are compiled automatically by GraphCor when a line of correlation (LOC) is saved during the graphing process. These files consist of the end points of the graphs and the end points of the LOCs. It is these numbers that define the ranges on the *X* and *Y* axes of all taxa from each section. The maximum FOs and LOs are calculated from the occurrences of ranges of each species in all sections.

Composite Range Data Files.—

These files are lists of species and their maximum range end points in mega-annums. They are compiled by GraphCor from the section files and the LOC files. The lists resulting from the combined three projects, MIDK3, MIDK4, MIDK41, and MIDK42, are saved as MIDK42CS.1; a copy for editing by the CORB working group is MIDK42CS.2. In this file names are changed to account for new generic assignments, species synonomies, and range alterations. The "look-up" tables show which section controls the range end points. Some age interpolations are unreasonable in comparison to published reports, so second or even third events have been selected as the new, revised FOs or LOs. CORB project specialists have collaborated in making these evaluations.

Stage Definition and Numerical Age Calibration

A primary goal of compiling a Cretaceous composite database in 1994 was to calibrate it with a numerical time scale from the beginning. At that time the Harland et al. (1990) time scale was the most refined and utilized, so it was selected as the *X* axis. The first section to be graphed to this time scale was the El Kef Cenomanian–Turonian section in Tunisia, because the stage boundaries were well constrained by ammonites, planktic foraminifera, and nannofossils. Subsequent Cenomanian and Turonian sections were added to the MIDK database in order to constrain the fossil ranges. The database was extended by graphing older and younger sections in which the stage boundaries were also well constrained by fossils common to reference sections. Since 1995 Global Stratotype Sections and Points (GSSP) have been selected for many Cretaceous stages (Ogg et al., 2004), and these sections have been graphed into the MIDK composite database.

The Cretaceous time scale employed in the CORB project spans from the base of the Barremian Stage to the base of the Danian Stage (Fig. 2). The boundaries of the Cretaceous stages are defined by the same criteria recommended by Ogg et al. (2004) (Appendix 2). Middle and Upper Cretaceous stage boundaries are constrained in the MIDK42CS.1 database by GSSPs and sections under consideration as GSSPs. These or other references sections provide continuous and uniform sediment accumulation rates across stage boundaries. Next, numerous sections containing CORBs were graphed to this data set so that the ages of CORBs could be interpolated. The result is a testable data set that can be critically evaluated.

The base Aptian is defined at Gorgo a Cebara, Italy (MIDK.43) and Cassis, France (MIDK.69); the base Albian is defined at Tartonne, France (MIDK.57) and Pre-Guitard, France (MIDK.58); the base Cenomanian is set at Mount Rissou, Rosans, France (MIDK.24, GSSP); the base Turonian is set at the Pueblo, Colorado, section (MIDK.15B, GSSP); the base Coniacian is at the Forwark Quarry, Poland, section (UPK.21) and the Salzgitter–Salder Quarry, Germany, section. The latter is incorporated into the Turonian–Coniacian composite standard of northern Germany (WOODCS.1). The base Santonian is at the Olazagutia Quarry, Spain (UPK.3) (note that the range of *Cladoceramus undulatoplicatus* is incomplete); the base Campanian is at the Dallas, Texas, U.S.A., section (UPK.2); the base Maastrichtian is at the Tercis les Bains Quarry, France (UPK.12 and 13, GSSP). The base of the Paleocene Series and the Danian Stage is at the El Kef section, Tunisia (UPK.5, GSSP).

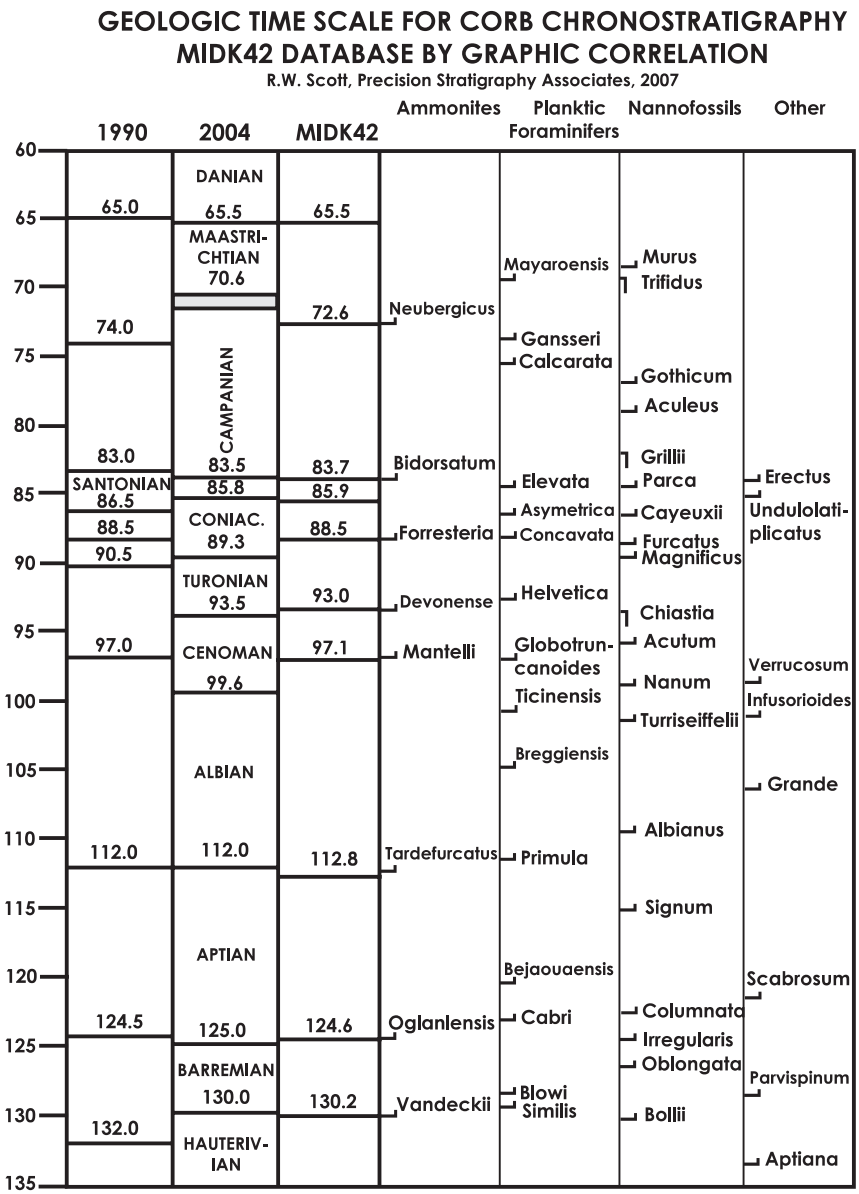

FIG. 2.—Geologic time scale used for the CORB project. The mega-annum scales of Harland et al. (1990) and Ogg et al. (2004) are compared to that of the MIDK42CS database. The first or last occurrences of key species in the MIDK42CS define stage boundaries.

The mega-annum ages of these stage boundaries are calibrated by interpolation with well-dated bentonites and magnetochrons, where present. The published time scale was recalibrated in 1995 and again in 1998 as new data were discovered and interpolations were made. The most recent time scale of Gradstein et al. (2004b) incorporates most of these changes; however, these authors note that the age calibrations of some Cretaceous stage boundaries are not yet definitive. For example, the base Maastrichtian at 70.5 Ma (Ogg et al., 2004, p. 365) was an arbitrary choice of two possible ages based on indirect correlations. The GSSP in the Tercis section at 115.2 m (Odin and Lamaurelle, 2001a, 2001b) is older at 72.0 Ma by graphic correlation with the MIDK41 range database. Also the age of the Albian–Cenomanian boundary is uncertain. The age in the 2004 scale of 99.6 ± 0.9 Ma is based on radiometric dates on tuffs interbedded with foraminifera and ammonites in Japan (Obradovich et al., 2002). The date of 97.13 Ma in MIDK42CS is based on correlating cosmopolitan dinoflagellates and sequence boundaries with the Clay Spur bentonite in the U.S. Western Interior radiometrically dated at 97.17 ± 0.69 Ma (Oboh-Ikuenobe et al., 2007). In order to recalibrate the MIDK database with new ages, especially for the Cenomanian–Turonian stage, the MIDK41CS.1 database was graphed to key sections spanning that boundary to shift its age from 90.5 to 93.00 Ma. This experiment resulted in the MIDK42CS.1 database, which sets the ages of fossils in the CORB sections (Appendix 3).

Nannofossil and Planktic Foraminifera Zones

The planktic foraminifera and nannofossils are stratigraphically useful groups in the Cretaceous System. Comprehensive zonal schemes have been revised for Lower (Bown et al., 1998)

and Upper Cretaceous (Burnett, 1998) nannofossils and for planktic foraminifera (Premoli Silva and Sliter, 2002). Their FOs and LOs have been integrated together (Bralower et al., 1995; Hardenbol and Robaszynski, 1998). The graphic correlation experiment was reasonably successful in replicating these schemes. The order and interpolated ages of planktic foraminifer zonal markers are generally consistent with previous reports (Fig. 3). However, some maximum nannofossil bioevents are either older or younger than predicted by these schemes (Fig. 4). First-appearance datums younger than expected and last-appearance datums older than expected are probably the result of insufficient sections in the MIDK database controlling the ages. But FOs that are older than expected and LOs younger than expected were reexamined to evaluate identifications, species concepts, reworking, or even placement of the position of unconformities. This examination resolved some of the discrepancies. Other differences may indeed be the result of longer ranges than reported.

Benthic Foraminifera Zones

Agglutinated benthic foraminifera are characteristic and diagnostic of Upper Cretaceous strata particularly where calcareous fossils are absent. However, the ranges of these species are not well integrated with either calcareous fossils or magnetochrons because they occur together in few sections (Kuhnt, 1990). Because agglutinated benthic foraminifers are stratigraphically important, a number of zonal schemes have been proposed

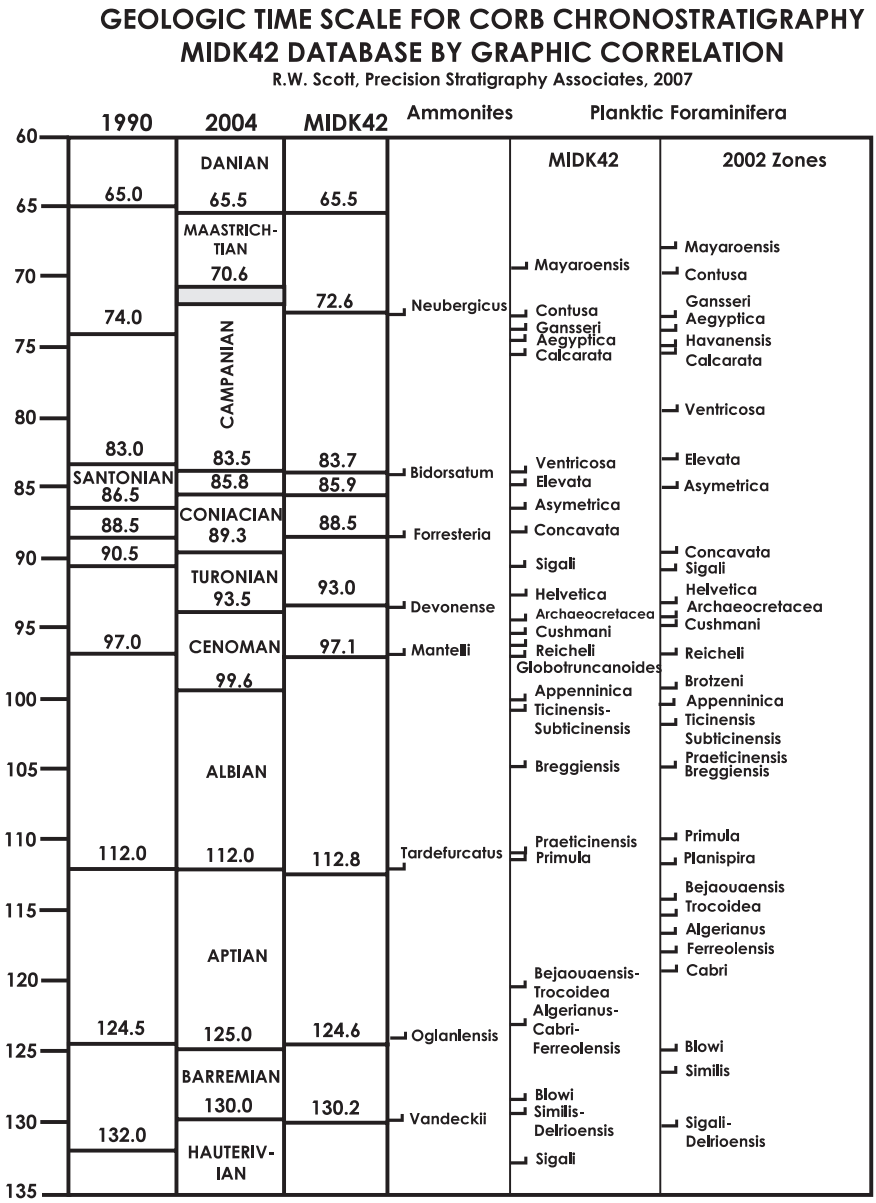

FIG. 3.—Geologic time scale of key planktic foraminifera in the MIDK42CS database calibrated to mega-annums. Bioevents are calibrated to the MIDK42 scale, not to other time scales, so the ages of the events do not match the stage boundaries. FOs of key species by Premoli-Silva and Sliter (2002) are plotted for comparison.

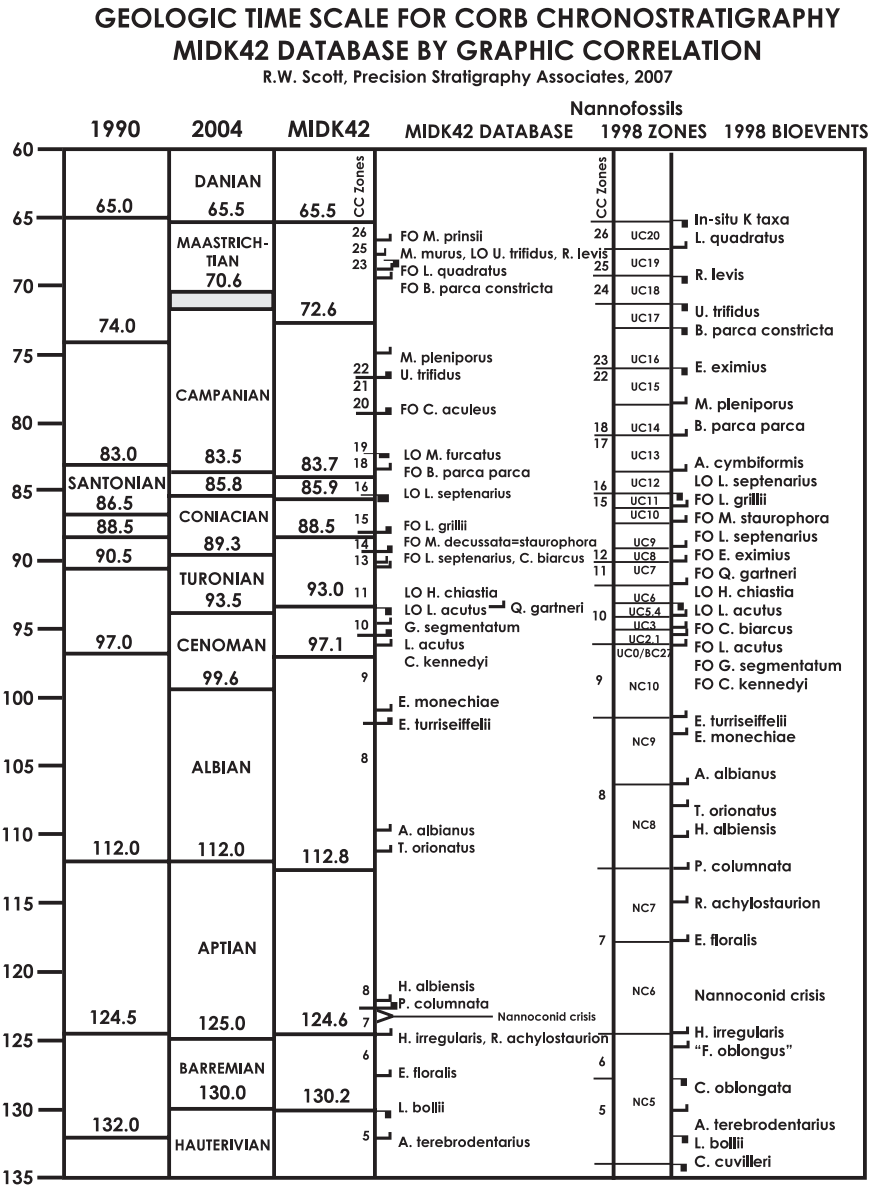

FIG. 4.—Geologic time scale of key nannofossils in the MIDK42CS database calibrated to mega-annums. The Tethyan zones defined by Burnett (1998) and the datums of the key taxa are compared with the ranges in MIDK42CS. Data tables of key fossil groups are accessible at www.precisionstratigraphy.com.

(Morgiel and Olszewska, 1981; Geroch and Nowak, 1983; Moullade et al., 1988; Neagu, 1990; Kuhnt, 1990; Bak, 2000).

Benthic foraminifera are present in many CORBs, including DSDP 603, 398, and 385, and ODP 641 (Fig. 5; Table 1). In the Bottacione Gorge section benthic foraminifera co-occur with Turonian–Maastrichtian planktic fossils (Kuhnt, 1990). Agglutinated benthic foraminifers in ten cores and outcrop sections are integrated by graphic correlation with ammonites, calcareous planktic foraminifers, nannofossils, magnetochrons, and radiometric dates in the MIDK42CS.1 data base. Three range zones are defined in the data base by the FOs of three common species: *Uvigerina jankoi* Majzon, *Caudammina [Hormosina] gigantea* Geroch, and *Goesella rugosa* (Hanzlikova). The FO of *Uvigerina jankoi* in Lower Turonian is slightly older than the FO of *Haplophragmium lueckei*, which has been used as a marker for a Turonian zone. The FO of *U. jankoi* is as old as the FO of *Praecystammina globigerinaeformis* Krasheninnikov, which is the name species of a mainly Coniacian zone. The FO of *C. gigantea* is slightly older than the Coniacian–Santonian boundary (86.36 Ma v. 85.91 Ma). The base of *G. rugosa* is in the upper part of the Campanian at 77.11 Ma, but its range is controlled by a single section. A fourth zone, *Haplophragmium problematicum* Neagu (also placed in *Bulbobaculites*), is not separated from the base of the *U. jankoi* Zone because it is not in any of the older sections in this database; its range is incomplete. New data reported by Skupien et al. (this volume) suggest that some ranges will be modified.

CORB SECTIONS DATABASE

Members of the IGC Project 463 team provided data of twenty-five key sections spanning CORBs (Fig. 6; Table 2). CORBs in seven other sections were dated by traditional zonation schemes. Additional sections were found in published records. The ages

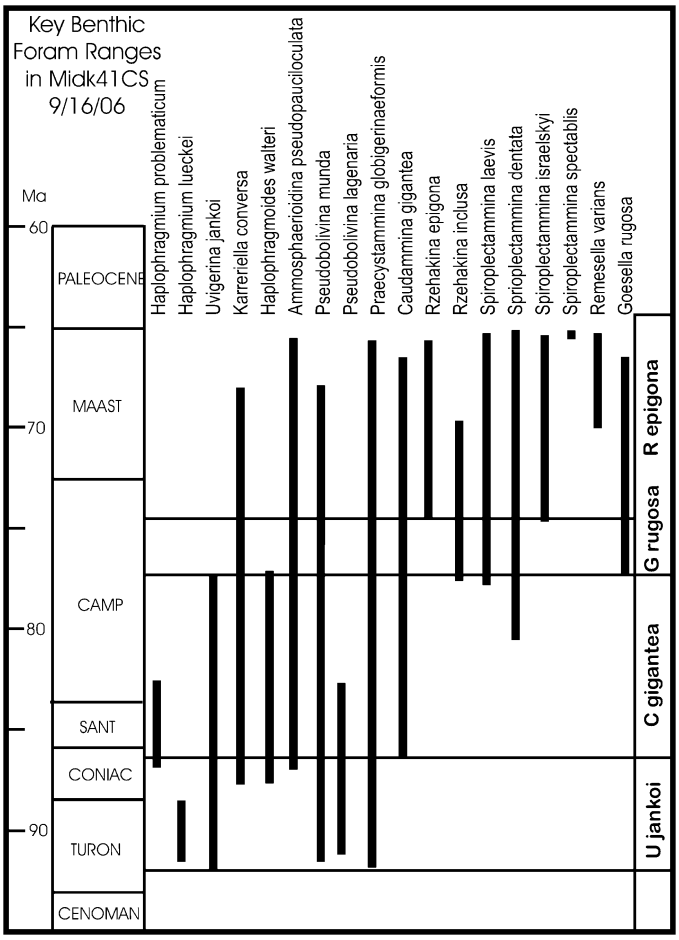

FIG. 5.—Ranges of key benthic forams.

and rates of sediment accumulation of selected sections of Cretaceous oceanic red beds were determined by graphic correlation experiments. The numerical ages of the first (FO) and last (LO) occurrences of each taxon or non-biotic chronostratigraphic event in the MIDK4 range database were measured by graphic correlation interpolation (Appendix 3).

In many sections black shale beds defined the Cenomanian–Turonian OAE 2, but black shales of the Coniacian–Santonian OAE 3 are not in the project. Beds of OAE 3 are localized primarily in the eastern Atlantic offshore of West Africa (de Graciansky et al., 1987; Hofman et al., 2003) and in the western Atlantic off the Demerara Rise (Friedrich and Erbacher, 2006). Ocean sections with this marker were graphed into the database. The correlation chart shows four general intervals of CORB deposition. (1) Albian–Cenomanian deposition of oceanic red beds was localized in separate basins and for brief durations. (2) Red-bed deposition began very soon following the OAE 2 event in the North Atlantic and in a few other basins, but lagged in others, such as off the east coast of northeastern South America, where oxygenated bottom waters developed in the middle Campanian (Friedrich and Erbacher, 2006). (3) In the North Atlantic and in some Carpathian basins CORB deposition persisted from the Turonian to the Maastrichtian, lasting even into the Paleogene in places. In many North Atlantic sections the top of the Cretaceous is an erosional surface overlain by Neogene strata. (4) In some basins a brief period of red-bed deposition occurred, and in other basins red beds alternate with gray and green beds, suggesting climatic control. CORB deposition was not a single, well-constrained, globally synchronous event. To evaluate patterns of red-bed deposition in more detail, lithologic sections in separate basins must be correlated.

APPLICATIONS

North Atlantic Transect

CORB strata are widespread in the North Atlantic and have been cored in numerous DSDP and ODP wells. CORBs

TABLE 1.—Ranges in Ma of key benthic forams in MIDK42CS.1, number of occurrences and sections that set the FO and LO.

TAXON	FO	LO	#	Sections
Ammosphaeroidina pseudopauciloculata	86.92–65.57	2	UPK22	UPK18
Bulbobaculites problematicus		85.08–84.16	1	CORB398D
Also as:				
Haplophragmium problematicum	86.92–82.35	2	UPK22	UPK18
Caudammina [Hormosina] gigantea	86.36–65.40	7	CORB603B	CORB398
Goesella rugosa	77.11–66.47	1	CORB398D	
Haplophragmium lueckei	91.62–88.55	2	CORB641A	CORB603B
Haplophragmoides walteri	87.67–77.07	1	UPK22	
Karreriella conversa	87.67–68.03	5	UPK22	CORB385
Praecystammina globigerinaeformis	92.96–65.57	8	CORB14	UPK18
Pseudobolivina gr. munda_lagenaria	91.19–82.71	1	CORB603B	
Pseudobolivina munda	91.63–67.94	8	CORB641A	UPK18
Remesella varians	70.03–65.35	1	UPK18	
Rzehakina epigone	74.44–65.56	5	CORB398D	UPK24
Rzehakina inclusa	77.38–69.74	2	CORBCOVA	CORB385
Spiroplectammina dentate	80.51–65.28	5	UPK17	DSDP515F
Spiroplectammina israelskyi	74.74–65.35	1	UPK18	
Spiroplectammina laevis	77.83–65.35	2	UPK18	UPK18
Spiroplectammina spectabilis	65.52–56.59	1	DSDP515F	
Uvigerinammina jankoi	91.96–77.21	10	CORB14	CORB398D

UPK17 = Casamanche corep; UPK18 = Botaccione Gorge; UPK22 = Hacho de Montejaque, Spain;
UPK24 = Rotwandgraben, Austria; CORB14 = Zasadne, Poland

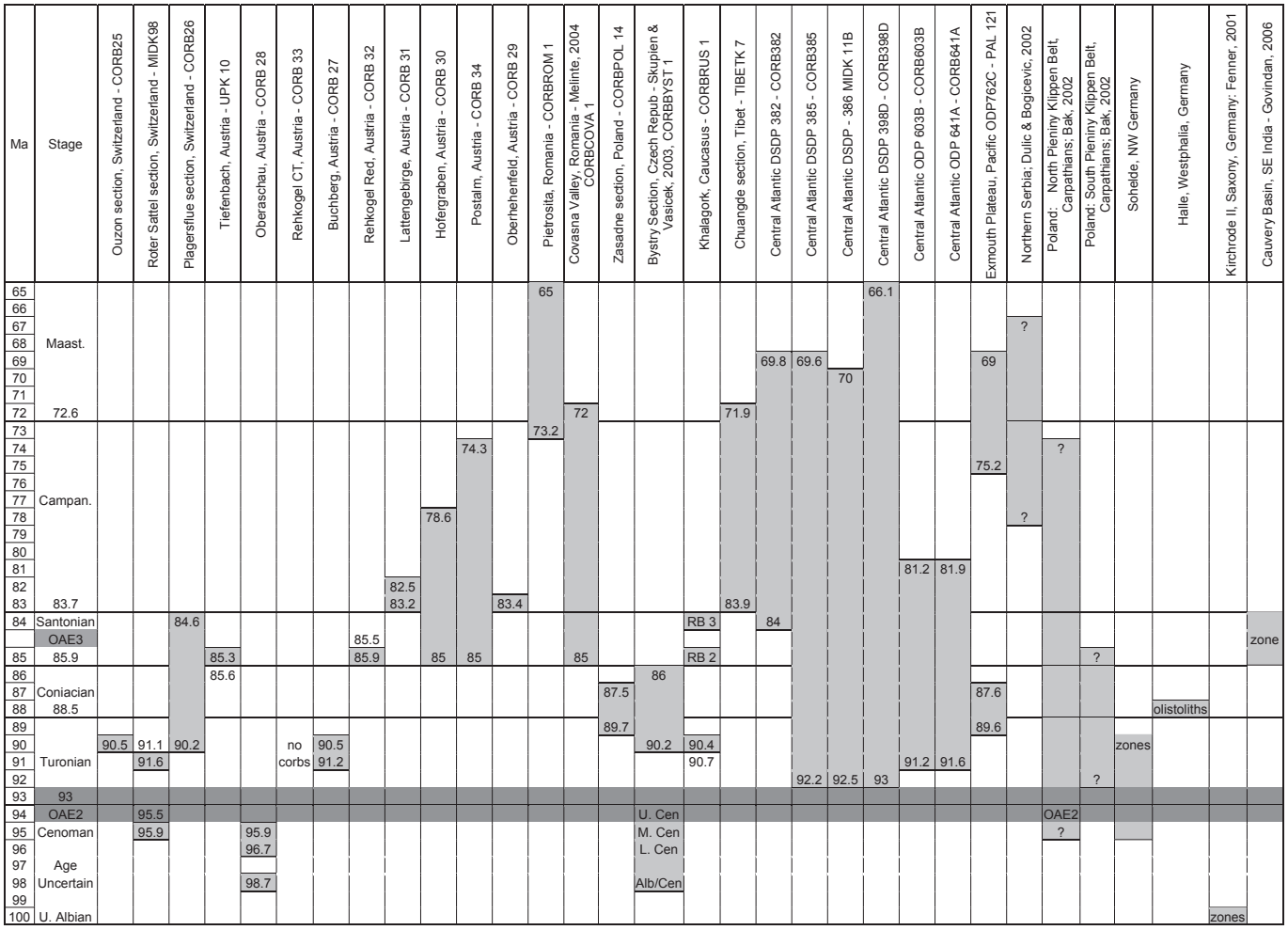

FIG. 6.—Chronostratigraphic chart of 25 CORB sections graphed to the MIDK42CS database. Seven sections on right side are plotted by zones only.

are common in the Turonian to Maastrichtian Plantagenet Formation, which is from 52 to 152 m thick in the cores of this cross section. CORB deposition followed the basin-wide oxygen-minimum OAE 2, which spanned the Cenomanian–Turonian boundary. Six core holes were graphed to the CORB database in order to date and measure rates of sediment accumulation (RSA). These strata are correlated in an east-to-west section from the continental shelf west of Iberia to the continental slope of North America (Figs. 7, 8). High-quality biostratigraphic data of planktic and benthic foraminifera, radiolaria, and nannofossils have been published by the Ocean Drilling Program.

The Plantagenet Formation overlies the Hatteras Formation, which is composed of uppermost Cenomanian organic-rich clay of OAE 2 (de Graciansky et al., 1987; Hu et al., 2005b). Core examination suggests that the Plantagenet Formation was deposited continuously from the Turonian to the Maastrichtian (W. Kuhnt and L. Jansa, personal communication, 2006). So the graphic interpretations show no hiatuses; however, significant changes in RSA are proposed. These changes partly correspond with two radiation events of benthic foraminifera (Kuhnt et al., 1996), one in the Turonian–Santonian and the second in the Campanian–Maastrichtian.

The Plantagenet Formation is generally sparsely fossiliferous and yields only agglutinated benthic foraminifera in its lower part, whereas in its upper part planktic foraminifera and nannofossils are sparse. Benthic foraminifera are calibrated by co-occurring planktic fossils in numerous published sections and define Turonian–Maastrichtian range zones, interval zones, or acme zones (Kuhnt et al., 1996). The ranges of the calcareous fossils are incomplete in most cores, so accurate first and last occurrences are lacking. The benthic foraminifer zones are well developed in DSDP 398D, where two benthic radiation events are recognized (Kuhnt et al., 1996). The first radiation followed OAE 2 and is dated by graphic correlation from the Turonian to the Santonian in DSDP 398D. No calcareous fossils are present in this lower interval in 398D (lithologic unit 3B). The second benthic foraminifer radiation event in 398D (unit 3A) ranges from Campanian to Maastrichtian, 77.20 to 66.10 Ma, and followed the Santonian anoxic event in the West African basins (de Graciansky et al., 1987). Calcareous foraminifera and nannofossils are moderately diverse in this interval. These two periods are present in other cores in the Atlantic, the Mediterranean, and the Pacific and represent widespread oxygenated deep-water conditions that are evidenced by both benthic foraminifer assemblages and CORBs (de Graciansky et al., 1987; Kuhnt et al.,

TABLE 2.—Basic CORB data for each section analyzed by graphic correlation.

SECTION	CORB POSITION meters	THICKNESS meters	STAGE	AGE Ma	OLD Ma	DURATION Myr	YOUNG Ma	RATE mm/yr	RATE cm/kyr	BEDDING TYPE	CYCLE BED THICKNESS cm	CYCLE DURATION kyr	PUBLISHED PALEO DEPTH m
DSDP398D upper	886.70–795.44	91.26	CAMP–MAAST	77.2–66.1	77.2	11.1	66.1	8.22	0.822	red/gray mdst	10–100	8.2–82	Above CCD
DSDP398D lower	947.75–886.70	61.05	TUR–CAMP	93–77.2	93	15.8	77.2	3.86	0.386	red/gray mdst	10–100	3.9–39	Above CCD
DSDP386	724.3–632.0	92.3	TUR–MAAST	92.50–70.00	92.5	22.5	70	4.1	0.41	Homogeneous & brown/yellow clay	NA	NA	NA
DSDP385	283.4–205.8	77.6	TUR–MAAST	92.20–65.50	92.2	26.7	65.5	11.59	1.159	red/gray clay & yellow brown/gray brown clay	~ 1	1.16	Above CCD
DSDP382	385.3–351.5	33.8	CAMP–MAAST	74.14–69.80	74.14	4.34	69.8	> 8.77	> 0.877	red clay/brown nanno ooze	2.0–20.0	8.8–88	Below CCD
ODP641A	53.55–1.5	52.05	TUR–CAMP	91.63–81.90	91.63	9.73	81.9	5.35	0.535	brown/ red brown clay	10.0–30.0	1.66–16.6	Below CCD
DSDP603B	1119.1–1024.28	94.82	TUR–SANT	91.20–81.20	91.2	10	81.2	9.48	0.948	red/gray clay	NA	NA	Above CCD
ODP762C upper	701–603.5	97.5	CAMPANIAN	75.25–69.90	73.25	5.35	69.9	50.77	5.077	brown/gray	35–135	178–685	1000
ODP762C lower	810.5–775	35.5	TUR–CON	89.63–87.60	89.63	2.03	87.6	17.24	1.724	red/gy marl	7 to 85	12–147	
ZASADNE	0–33	33	TUR–SANT	92.2–84.2	92.2	8	84.2	4.12	0.41	Homogeneous	NA	NA	Abyssal
TIEFENBACH	44–50	6	SANTONIAN	85.56–85.33	85.56	0.53	85.33	19.6	1.96	Homogeneous	NA	NA	Outer Shelf
COVASNA	250–280	30	MAAST	72.2–69.94	72.2	2.26	69.94	13.48	1.35	Homogeneous	NA	NA	Abyssal
PIETROSITA	20–85	65	CAMP–MAAST	72.72–63.6	72.72	9.12	63.6	7.14	0.7	red/gray marl	~ 5.0–20.0	~ 3.5–14	200
BYSTRY	25–306	281	CEN–SANT	94.7–83.85	94.7	10.85	83.85	78.14	7.8	red/gray shale	Unknown	NA	NA
KHALAGORK	146–154	8	TURONIAN	90.72–90.37	90.72	0.35	90.37	22.34	2.23	Thin ls	10.0–15.0	22.3–33.5	abv CCD
CHUANGDE	410–382	28	CAMPANIAN	83.7–73.2	83.7	10.5	73.2	2.66	0.27	homog shale			abv CCD
BUCHBERG	0–7	7	TURONIAN	91.9–89.55	91.9	2.35	89.55	3	0.3	marl/ls	20 & 75	6 & 22.5	abv CCD
OBERASCHAU	6.23 to 41.05	5 laminae	ALB–CEN	98.7–95.87	98.7	2.83	95.87	12.4	1.24	sh/turbidites	< 20	< 20	abv CCD
OBERHEHENFELD	0–2	2	CAMPANIAN	83.4–82.9	83.4	0.5	82.9	~ 4	~ 0.4	marl/ls			abv CCD
HOFERGRABEN	0–40	40	SANT–CAMP	85.0–78.55	85	6.45	78.55	9.1–5.1	0.91–0.51	marl/ls/turbid			abv CCD
LATTENGEBIRGE	52.7–66.5	13.8	CAMPANIAN	83.2–82.5	83.2	0.7	82.5	19.6	1.96	marl/ls			abv CCD
REHKOGEL RED	0–11	11	SANTONIAN	85.9–85.5	85.9	0.4	85.5	28.5	2.85	marl/ls			abv CCD
REHKOGEL CT	0–5.2	5.2	CEN–TUR	96.5–89.82	96.5	6.7	89.82	0.8	0.08	marl/ls			abv CCD
POSTALM	3–180	177	CAMPANIAN	83.7–74.3	83.7	9.4	74.3	18.83	1.88	marl/ls			abv CCD
OUZON lower	11.2–19.6	< 8.4	U APTIAN	118.3–116	118.3	< 2.3	116	3.7	0.37	CORB bed in pelagic wkst	50–100	18.5–37	abv CCD
OUZON middle	19.6–27.1	< 7.5	ALBIAN	111.9–102	111.9	9.9	102	0.8	0.08	wkst–marl	10 to 60	0.8–4.8	abv CCD
OUZON upper	64.4–65.5	1.1	TURONIAN	90.44–90.4	90.44	0.04	90.4	3.25	0.32	pelagic wkst	10	3.2	abv CCD
ROTER SATTEL lower	51–53.5	2.5	CENOMAN	95.85–95.75	95.85	0.1	95.75	25	2.5	pelagic wkst	10	25	abv CCD
ROTER SATTEL upper	64–68	4	TURONIAN	90.69–89.73	90.69	0.96	89.73	4.17	0.42	pelagic wkst	10	4.2	abv CCD
PLAGERSFLUE	0–30	30	TUR–SANT	90.2–84.6	90.2	5.6	84.6	5.36	0.54	pelagic wkst	10 to 20	5.4–10.8	abv CCD
TOTALS						197.39		405.4	40.54				
MEAN						6.58		13.51	1.35				
RANGE						0.04–26.7		0.8–78.14					

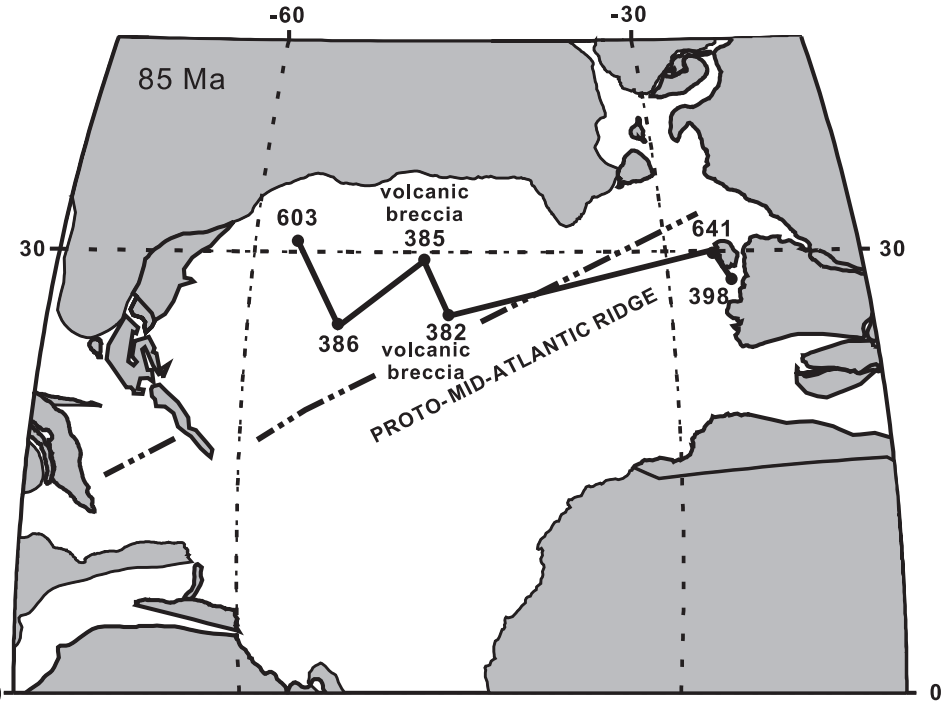

FIG. 7.—Late Cretaceous North Atlantic paleogeographic map showing positions of six DSDP/ODP core holes penetrating marine red beds and correlated by graphic correlation. The map was downloaded from the ODSN Plate Tectonic Reconstruction Service website (www.odsn.de).

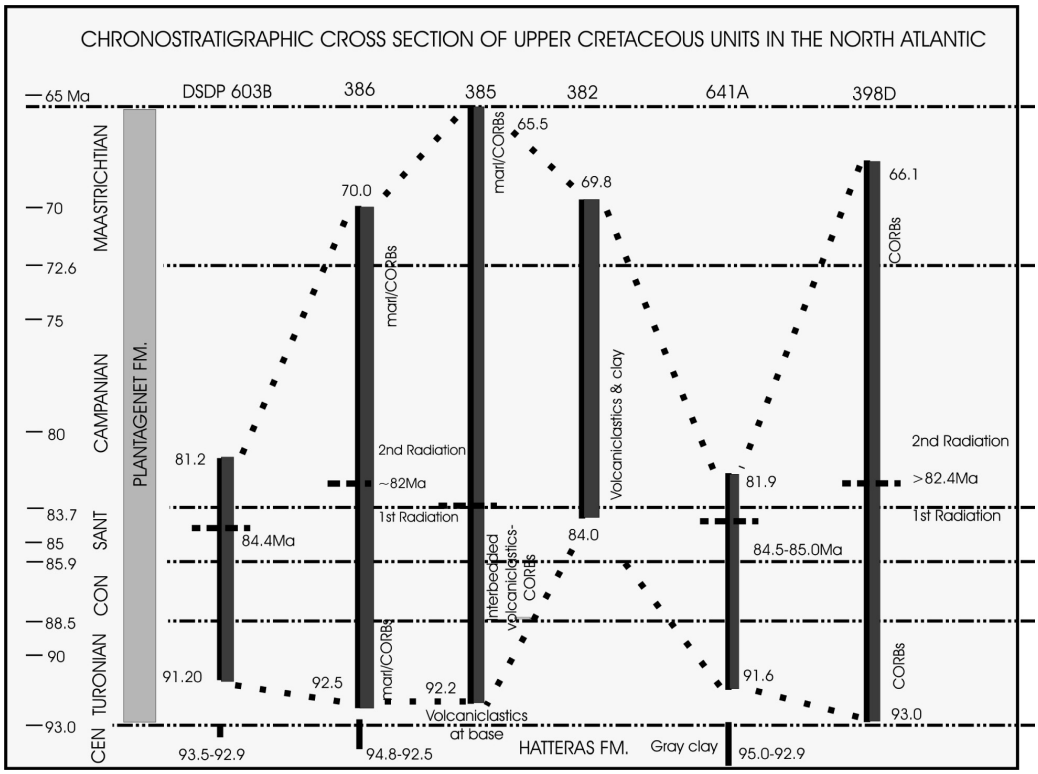

FIG. 8.—North Atlantic cross section of six core holes shows chronostratigraphic correlation of CORBs in the Plantagenet Formation. "First radiation" and "second radiation" of benthic foraminifer events (Kuhnt et al., 1996) are separated by heavy dashed lines. Ages are interpolated by graphic correlation. Top of Cretaceous sections are truncated by Cenozoic unconformity.

1996). In the Campanian, oxygenated bottom waters appeared along the northeastern coast of South America (Friedrich and Erbacher, 2006). Clearly, during the Campanian–Maastrichtian in the North Atlantic, the carbonate compensation depth (CCD) was deeper than during the older event. Possibly deep-water pH and the depth of the CCD were related to more submarine volcanism during the Turonian–Coniacian than later. Volcaniclastic breccias below CORBs at sites 382 and 385 are radiometrically dated at 79 ± 4 Ma to 91.2 ± 3 Ma (Houghton et al., 1979).

The Turonian to basal Santonian CORB interval was graphed in five wells (Fig. 8). In DSDP 603B red and brown claystone beds 10–20 cm thick are interbedded with greenish gray thinly laminated clay and silt turbidites and greenish gray claystone. Claystone is composed mainly of smectite with some kaolinite and illite, all of which were transported from the nearby continent (Huff, 1987; de Graciansky et al., 1987). Two intervals with very diverse foraminifera are separated by a low-diversity upper Santonian section. The top of the Plantagenet Formation is capped by a lamina of dark green smectite spherules that are interpreted to be remnants of impact ejecta from an extraterrestrial object at the end of the Cretaceous (Klaver et al., 1987). In DSDP 386, the type section of the Plantagenet Formation, dark red-brown claystone with local dark green-gray laminae disconformably overlies organic-rich clay of OAE 2. This grades up into red claystone with green-gray laminae that is overlain by homogeneous red claystone composed of illite, mixed-layer clay, kaolinite, chlorite, quartz or chalcedony, feldspar, and Fe–Mn oxides. The Crescent Peak Member is a thin limestone bed at top. The shift in benthic foraminifer diversity at about -690 to -680 mbsf is close to the top of the Santonian. In DSDP 385 core, red-brown silty clay with basalt clasts grades up into dark brown sand and volcaniclastic breccia overlain by mottled yellow-red silty clay and interspersed green-gray sand laminae. The overlying Maastrichtian Crescent Peak Member is brown, yellow-red, and green gray nannofossil ooze. It appears that both foraminifer radiations are recorded in this well, although Kuhnt et al. (1996) plotted the entire interval in the second radiation. However, the lower two cored intervals from about -283 to -269 mbsf are dated as Turonian–Santonian both by benthic foraminifer zones (Kuhnt et al., 1996) and by graphic correlation. So the older radiation event is also recorded in this core hole.

In DSDP 382 the Plantagenet Formation is composed of dark brown-red claystone with silt and marl laminae (Fig. 8). Iron oxides and magnetite are very abundant. At the base of the formation a bed of silty red clay 1.4 m thick overlies volcaniclastic breccia and sandstone. *Broinsonia parca parca* in this basal red clay dates it as no older than Lower Campanian, about 84 Ma. Thus this interval is coeval with the second foraminifer radiation event, although the benthic foraminifera are not reported in core 382. However, the calcareous fossils are moderately diverse. The top of the Plantagenet is Lower Maastrichtian, dated at 70.30 Ma, and is disconformably overlain by Miocene clay. In ODP 641A a unit about 52 m thick is gradationally interbedded reddish brown and grayish brown clay in laminae 10–20 cm thick. The transition between benthic foraminifer radiation events one and two is between -19 and -12 mbsf in this interval, and it is correlated with the Santonian–Campanian boundary by graphic correlation. CORB deposition began in the eastern Atlantic within 670 kyr following the Cenomanian–Turonian anoxic event. Black clay of OAE 2 was deposited between 93.53 Ma and 93.07 Ma in the MIDK42 chronostratigraphic database. The overlying green clay at the base of the Plantagenet may represent a condensed interval, and CORB deposition began no later than 92.30 Ma, on the basis of the ages of the benthic foraminifera. In DSDP 398D the Plantagenet disconformably overlies Cenomanian black claystone and gray-green calcareous mudstone. A lower lithologic interval (unit 3B) of red to yellow-brown mudstone and interbedded silt laminae is overlain by an upper interval (unit 3A) of red to brown marly chalk and claystone that spans the Cretaceous–Paleocene boundary. The boundary between the two radiation events is between -890 and -900 mbsf. Graphic correlation projects this interval in the lower Campanian. However, the plot suggests that a hiatus may be present at -886.7 mbsf, so that an alternative LOC would date the first radiation older than basal Campanian. This core interval should be reexamined for evidence of a depositional break.

High-precision correlation of the Plantagenet Formation in six cores in the North Atlantic date two lithologic intervals and their foraminifer assemblages that represent two distinct deep water masses (Fig. 8). Deposition of the Turonian–Santonian interval began immediately following OAE 2 and continued until about 84 Ma. Benthic foraminifera diversified and red beds were deposited in this oxygenated water mass. The CCD was relatively shallow because calcareous fossils were not preserved. North Atlantic submarine volcanism is indicated by volcanic breccia interbedded with Turonian–Santonian clay at site 385 and with Campanian clays at DSDP site 382; submarine volcanic effluents may have affected the depth of the CCD. The younger water mass developed during the Campanian to Maastrichtian, when benthic foraminifera again diversified and calcareous fossils were preserved, so the CCD was relatively deeper. Red marine clays and turbidites alternated with gray and green beds. Rates of sediment accumulation generally were lower during the Turonian–Santonian interval than during Campanian–Maastrichtian time. Rates during the older period averaged 4.85 m/Myr and during the younger interval averaged 7.61 m/Myr, when carbonate was deposited with clay. In comparison, de Graciansky et al. (1987) estimated that in the 386 and 398D wells the Turonian–Santonian accumulation rate was about 3.3 m/Myr and the Campanian–Maastrichtian rate was about 5.7 m/Myr.

Pre-Alps of Switzerland

Aptian–Santonian CORBs are exposed in nappes of the Romandes and Chablais Pre-Alps in southwestern Switzerland (Fig. 9). This sedimentary succession, up to 100 meters thick, was deposited in a basin of the Briançonnais domain on the northern margin of the Alpine Tethys Ocean (Strasser et al., 2001). Biostratigraphic data of three measured sections were graphed to determine the age and rates of sediment accumulation of CORBs in this basin. The Roter Sattel section in the Romandes Pre-Alps south of Fribourg yielded very high-resolution data (Strasser et al., 2001). The stratigraphy of the Ouzon section was documented by Hable (1997), and the Plagersflue section by Guillaume (1986).

The Aptian to basal Turonian intervals of the Ouzon and Roter Sattel sections correlate accurately by means of planktic foraminifera (Fig. 10). Aptian, Albian, and lowermost Turonian CORBs in the Ouzon section are relatively thin and are interbedded with marly mudstone, wackestone, and packstone with planktic foraminifera. The red planktic foraminifer limestone beds are 0.2 to 3 m thick. CORB deposition was intermittent beginning in the Late Aptian at about 116 Ma and ended in the Albian about 100 Ma. A brief 340,000 yr period of CORB deposition during the Turonian at about 90.5 Ma resulted in a thin-bedded wackestone unit 1.1 m thick. Above this bed are 14 more very thin red beds, each a few centimeters thick, that indicate that CORB deposition persisted intermittently into the Late Turonian. The estimated RSA was 3.2 m/Myr. At this rate beds

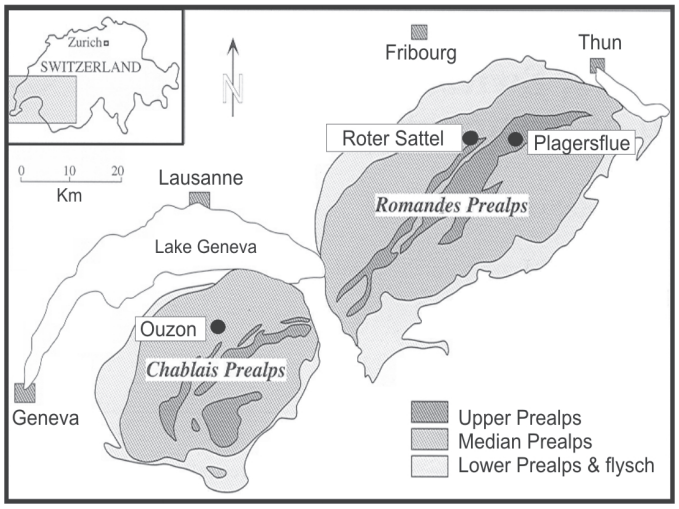

FIG. 9.—Map of Pre-Alps in Switzerland showing location of three CORB outcrop sections.

deposited during a 20 kyr precessional climatic cycle would be about 6–7 cm thick and beds of the obliquity frequency would be 12–13 cm thick.

About 70 km northeast of the Ouzon section in the Roter Sattel section Early Cenomanian CORB deposition began about 95.9 Ma and resulted in a 2.5-m-thick interval of thin-bedded foraminifer wackestone (Strasser et al., 2001). Red-bed deposition lasted about 610 kyr at a rate of 4.1 m/Myr. In the nearby Plagersflue section, CORB deposition persisted throughout the Turonian, Coniacian, and Santonian from about 90.2 Ma to 84.6 Ma. The CORB interval is the Rote Platte Formation and is bounded by submarine hardgrounds. Thin-bedded red wackestone alternates with light gray wackestone throughout this interval. The RSA was about 5.4 m/Myr. CORB strata in the Pre-Alps indicate that deposition of red marine limestone occurred at different times in different places for varying durations and at different rates.

Eastern Alps of Austria

A nearly complete record of Late Cretaceous deposition with marine red beds is exposed in the Eastern Alps. The interbedded siliciclastic and calcareous facies were deposited in the Penninic Ocean between two colliding plates (Faupl and Wagreich, 1992; Wagreich, 2006). A north-to-south stratigraphic cross section composed of nine outcrops extends from the stable southern margin of the European block (Helvetic, Ultrahelvetic, Rhenodanubian Flysch, and Penninic tectonic zones) to the Austroalpine microplate on the northern margin of the Apulian plate, exposed in the Northern Calcareous Alps (see Figure 1 in Wagreich, this volume). Planktic foraminifera and nannofossil biostratigraphy indicate that deposition was above the CCD. Biostratigraphic data of nine measured sections were graphed to the MIDK41 Database to test the ages and rates of sediment accumulation (RSA) of CORBs and associated turbiditic facies.

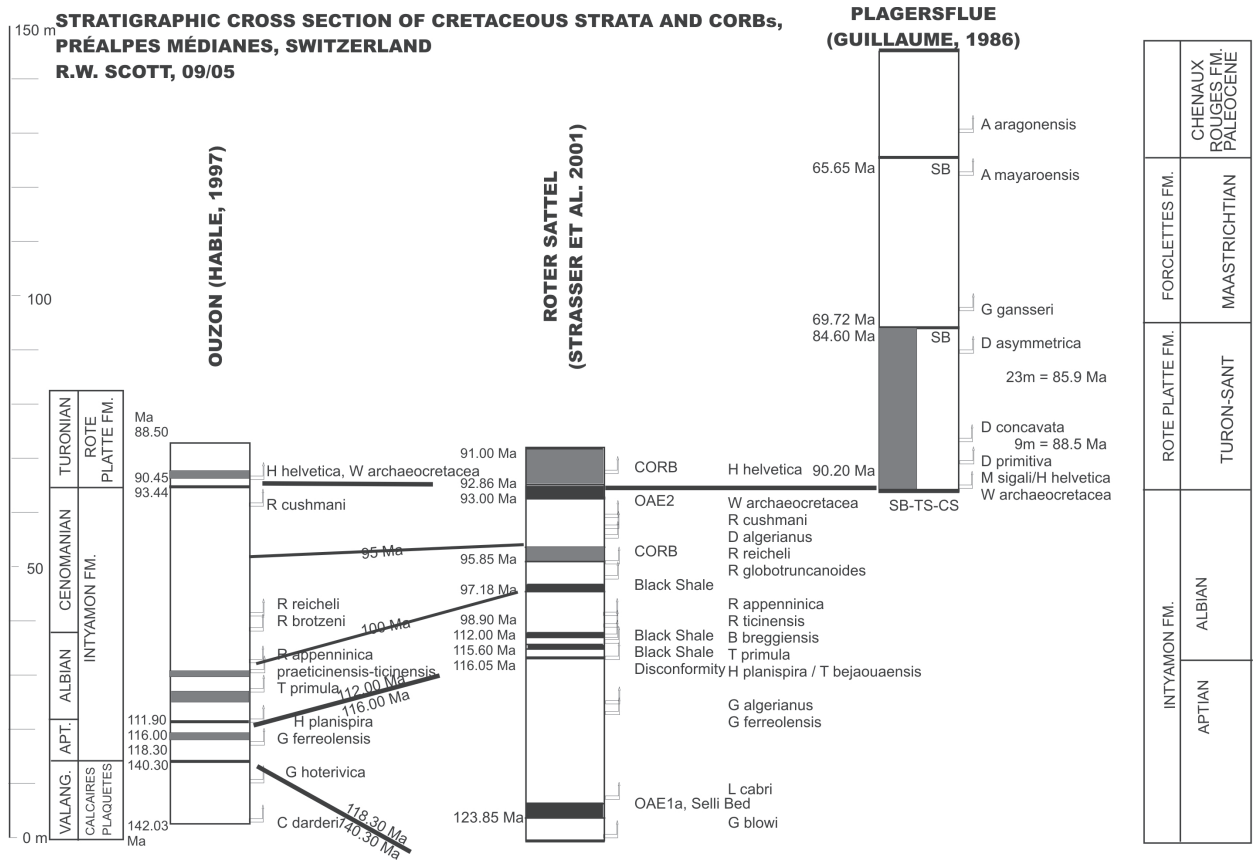

FIG. 10.—Chronostratigraphic cross section of marine red beds in Pre-Alps outcrops. Ages are interpolated by graphic correlation.

Timing and duration of CORB deposition varied at different places in this complex tectonic region. It was intermittent on the southern slope of the European Plate, recurring in Late Albian, Cenomanian, Turonian, Santonian, and Campanian times (Fig. 11). Depositional periods of marine red beds became longer from the Albian to the Campanian, and the RSA varied from site to site. Some red beds appear to record climatic forcing cycles. CORB deposition was mainly during transgressive periods when siliciclastic input was low and were controlled by tectonics and sea level (Wagreich, 2006). On the Austroalpine Microplate, CORB deposition was brief during the Santonian and spanned most of the Campanian, diminishing during the Maastrichtian (Wagreich and Krenmayer, 2005).

Albian and Cenomanian CORBs in the Helvetic, Ultrahelvetic, and Penninic tectonic zones are quite thin, up to 47 cm thick, indicating very brief events about 20 kyr in duration (Fig. 11, Oberaschau section 28). Two thin Upper Albian red marl beds underlie a thin organic-rich bed. The FOs of dinoflagellates and a nannofossil constrain the age of the black shale at 98.55 Ma, which is coeval with OAE 1c at the North Atlantic DSDP site 386. The age of this bed is projected to be from 98.9 to 98.2 Ma by graphic correlation. Three higher thin red marine beds span the Early to Middle Cenomanian from 96.72 to 95.87 Ma. The Cenomanian–Turonian anoxic event OAE 2 is recorded in the "Buntmergelserie" at Rehkogel CT (section 33). The graphic interpretation of the Turonian interval is constrained by correlation of the black shale with the carbon peak OAE 2 (93.5–92.9 Ma) in the Bonarelli bed in Italy and the FO of *Helvetoglobotrucana helvetica*, which predicts a RSA of 1.83 m/Myr. At this rate beds about 42 mm thick would represent the climatic precession frequency of approximately 23 kyr. The precession frequency is also reported in Cenomanian–Turonian marl–limestone cycles in the Western Interior (Sageman et al., 1998; Scott et al., 1998). In the Rehkogel section additional data are needed to test this hypothesis.

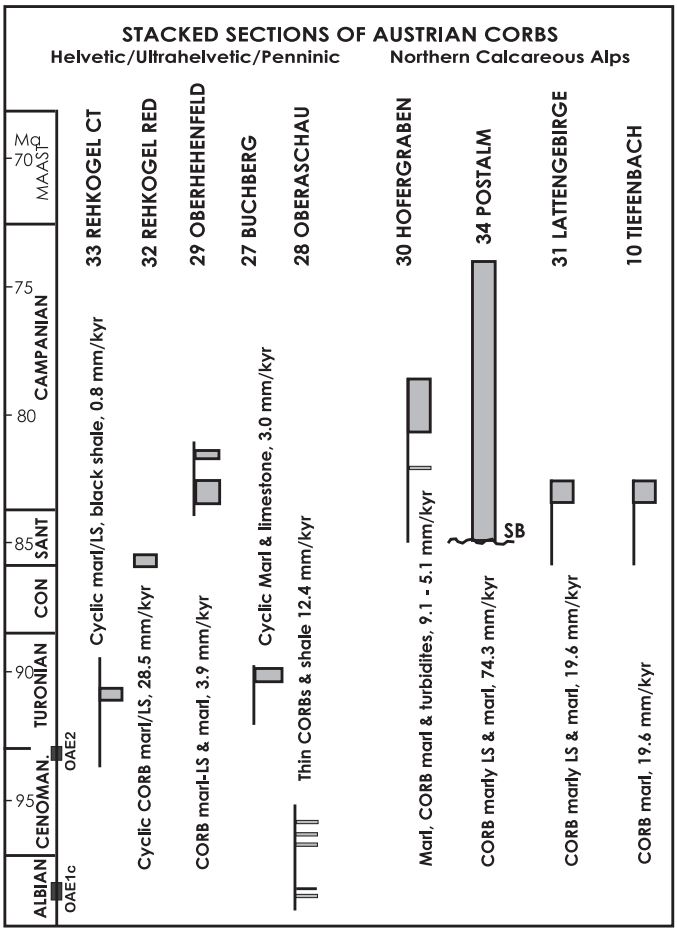

FIG. 11.—Chronostratigraphic cross section of eight CORB outcrops in Austria.

About 1.8 Myr after the end of OAE 2, Turonian CORB deposition became well established at Buchberg (Fig. 11, section 27) (Neuhuber et al., 2007). Gray limestone and marl are interbedded with red marl. Bed thicknesses range from 10 to 30 cm, and Neuhuber et al. (2007) suggested that deposition was influenced by the 23 kyr climatic precession cycle at a RSA of 7.4 m/Myr. In comparison, a graphic plot of the FOs of numerous planktic foraminifera and nannofossils predicts a RSA of 3.0 m/Myr, which suggests longer climatic frequencies of 42 and 100 kyr. Again, additional data will test these interpretations.

Santonian CORB deposition is recorded by thin-bedded marl–limestone cycles at Rehkogel Red (Fig. 11, section 32) of the "Buntmergelserie". The regular thickness of the bedding suggests that climatic forcing may have been a factor controlling deposition rates, but the RSA cannot be measured because the section is faulted (Wagreich, 2002). The Santonian red-bed interval in the "Buntmergelserie" is about 0.5 m thick at Oberhehenfeld (section 29), where it is overlain by gray shale capped by a Lower Campanian red-bed interval about 25 cm thick.

On the Austroalpine Microplate, Campanian CORBs are interbedded with gray marl in an interval nearly 180 m thick and were deposited on the slope during more than 10 Myr at Postalm–Retschegg (Fig. 11, section 34). Here the Campanian Bibereck Formation disconformably overlies Santonian conglomeratic sandstone. Slow deepening at the beginning of the Campanian deposited three meters of gray shale (Wagreich and Neuhuber, 2005). This grades up into medium- to thick-bedded, red argillic limestone and carbonate turbidites of the Nierental Formation. The Campanian nannofossil succession in the Nierental spans zones CC18 to CC23 (about 84 to 71 Ma). Graphic correlation narrows the time span to about 83.6 to 74.5 Ma. The RSA increased up section from about 11.6 m/Myr to 36.9 m/Myr and averaged 28.5 m/Myr, which is comparable to the rate of 25 m/Myr estimated by Wagreich (2002, p. 40). The graphic correlation experiment predicts that the precession cycles would be about 26–27 cm thick in the lower third of the section and about 85 cm thick in the upper part. The Lower Campanian CORB interval at Lattengebirge (section 31) is 13.8 m thick and ranges in age from 83.2 to 82.5 Ma. The predicted RSA ranges from 19.6 to 36.5 m/myr. In a partly coeval section of the Upper Gosau Subgroup at Hofergraben (section 30), thin red beds are interbedded with gray marl and sandstone–siltstone turbidites. The RSA of the lower part without red beds is 9.1 mm/kyr, and in the upper part with red beds it is 5.1 mm/kyr. These rates are significantly lower than at Lattengebirge.

RATES AND DURATIONS OF CORB ACCUMULATION

The duration of CORB deposition was generally shorter in epicontinental basins than in Atlantic oceanic basins. The duration of deposition in epicontinental basins ranged from 0.04 to 10.85 Myr and averaged 4.28 Myr (Fig. 12; Table 2). The duration of oceanic CORBs ranged from 2.03 to 26.7 Myr and averaged 11.95 Myr. Durations are exceptionally high in three North Atlantic sites, DSDP 385, 386, and 398D, where deposition was appar-

ently continuous from Turonian to Maastrichtian times (W. Kuhnt and L. Jansa, personal communication, 2006).

In contrast, the mean rate of sediment accumulation (RSA) in epicontinental basins tended to be similar to that in oceanic basins (Table 2). The RSA in epicontinental basins ranged from 0.80 to 78.14 m/Myr and averaged 13.62 m/Myr. In North Atlantic basins the rate ranged from 3.86 to 50.77 m/Myr and averaged 13.26 m/Myr. The higher rates are where CORBs are interbedded with turbidites. These mean rates are on the high end of rates of Holocene red clay, which range from 0.5 to 13 m/Myr during the past 10,000 yr (Enos, 1991). On the other hand, the mean rates of accumulation of Cretaceous red beds are the lower end of rates for Holocene bathyal and abyssal deposits (Enos, 1991). The RSA was exceptionally high in the Campanian at OPD site 762C and in the Bystry section, where turbidites are a major part of the deposits. This sample of CORB sections shows no significant changes in durations and rates from the Turonian to the Maastrichtian (Fig. 12).

Regularly interbedded CORBs were deposited at about the same mean duration as homogeneously bedded deposits: 6.77 Myr vs. 5.32 Myr (Table 2). The duration of regularly bedded CORBs ranged from 0.04 to 26.7 Myr, and the duration of homogeneously bedded deposits ranged from 0.53 to 10.5 m/Myr. In contrast, the mean rate of accumulation (RSA) of regularly interbedded CORBs was greater than that of homogeneously bedded deposits: 14.06 m/Myr vs. 9.97 m/Myr. The range of the rate of accumulation for regularly bedded deposits was much greater, from 5.99 to 68.2 m/Myr, than the rate for homogeneously bedded deposits, which ranged from 2.25 to 14.9 m/Myr. The greater RSA of interbedded deposits probably was the effect of input of calcareous pelagic and turbidite sediment. In comparison, in the U.S. Western Interior the RSA of Turonian–Santonian interbedded chalk and marl was approximately 24 m/Myr (Scott et al., 1998). Regularly bedded chalk deposits in England and Italy, where clay input was minimal, were deposited at mean rates of 15 and 12 m/Myr, respectively (Scholle et al., 1983).

Climatic forcing of CORB marl–limestone bedding cycles in Austria has been proposed (Neuhuber et al., 2007). The thicknesses of regularly interbedded red and gray mudstone or interbedded marl and limestone in the sampled sections vary from 1 cm to 100 cm (Table 2). Graphic correlation tests this hypothesis and provides ranges of cycle frequencies (Scott et al., 1998). In the Buchberg, Austria, section, Turonian gray limestone and marl alternate with red marl and limestone in cycles about 20 cm thick that are combined into longer-term cycles about 75 cm thick. Time-series analysis of total carbonate content resulted in productivity cycles 10 kyr and 20.7 kyr in duration (Neuhuber et al., 2007). The duration of red-bed deposition ranged from 30 to 360 kyr. Graphic correlation of the Buchberg section predicts a RSA of 3 m/Myr, so the 20 cm cycles represent 6 kyr and the 75 cm cycles are in the duration of 22.5 kyr, which is in the range of the precessional cycle as predicted by time-series analysis. The ranges of suggested cycle frequencies in other sections are quite variable, some of which are within the range of orbital frequencies and others are not. Each case should be fully evaluated to test the hypothesis that these cycles represent one of the orbital cycles. However, it is reasonable to consider that some CORB–marl cycles are related to climatic forcing.

CONCLUSIONS

The MIDK42CS.1 Cretaceous Chronostratigraphic Database was constructed by means of graphic correlation for the CORB Cretaceous time scale from published reports of 150 outcrops and cored sections. This database integrates the ranges of nearly 3000 taxa of planktic and benthic foraminifera, nannofossils, dinoflagellates, ammonites, inoceramids, magnetochrons, radiometric dates, geochemical events, and selected sequence stratigraphic markers in reference sections. Cretaceous stage boundaries from the Barremian to the Maastrichtian are defined in the database by GSSP sections or key reference sections. The boundaries are calibrated to radiometric dates.

Correlation of CORB sections show the following: (1) Albian–Cenomanian deposition of oceanic red beds was localized in separate basins and for brief durations. (2) Red-bed deposition began very soon following the OAE 2 event in the North Atlantic and in a few other basins but lagged in others. (3) In the North Atlantic and in some Carpathian basins, CORB deposition persisted from the Turonian to the Maastrichtian, lasting even into the Paleogene in places. In many North Atlantic sections the top of the Cretaceous is an erosional surface overlain by Neogene strata. (4) In some basins a single period of red-bed deposition occurred, and in other basins red beds alternate with gray and green beds, suggesting climatic control. CORB deposition was not a single, well-constrained, globally synchronous event.

High-precision correlation of the Plantagenet Formation in the North Atlantic date two lithologic intervals and their fora-

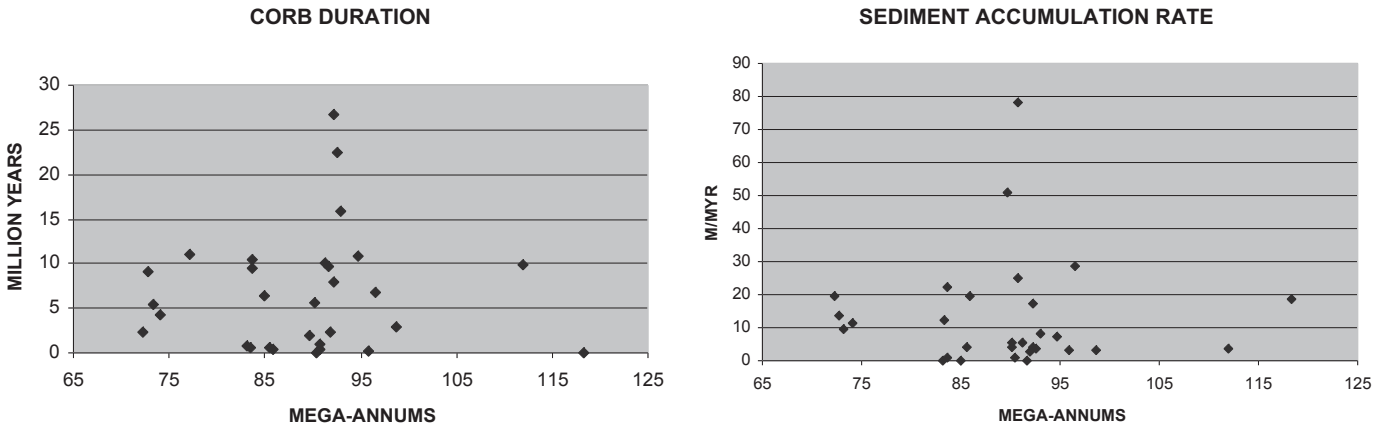

FIG. 12.—Graphs showing CORB durations and rates calculated by graphic correlation of sections in Table 1. **A)** Mean duration of CORB deposition plotted to the age of onset of deposition. **B)** Mean rate of sediment accumulation plotted against the age of onset of deposition.

minifer assemblages that represent two distinct deep water masses (Kuhnt et al., 1996). During deposition of the Turonian–Santonian interval, benthic foraminifera diversified and red beds were deposited in oxygenated waters. Deposition was below the CCD, and calcareous fossils were not preserved. Late Cretaceous submarine volcanism was widespread in the North Atlantic, and its effluents may have influenced the depth of the CCD. During the Campanian to Maastrichtian, benthic foraminifera again diversified and calcareous fossils were preserved, so the CCD must have been deeper than before. CORB strata in the Swiss Pre-Alps indicate that deposition of red marine limestone occurred at different times in different places for varying durations and at different rates.

The duration of CORB deposition generally was shorter in epicontinental basins than in oceanic basins. The average rate of sediment accumulation tended to be similar in epicontinental basins and in oceanic basins. Regularly bedded CORBs were deposited at about the same average duration as homogeneously bedded deposits, 6.77 Myr v. 5.32 Myr, but regularly bedded CORBs accumulated at a faster rate than homogeneously bedded deposits. Many repetitively bedded oceanic red beds were deposited at rates close to orbital frequencies; however, others were not. Each case should be fully evaluated to test the hypothesis that these cycles represent one of the orbital cycles. However, it is a reasonable hypothesis that some CORB–marl–limestone cycles are related to climatic forcing.

ACKNOWLEDGMENTS

Many colleagues in IGSP 463 contributed biostratigraphic data, either directly or through published data. Data for the North Atlantic transect and the Pacific core were published in several DSDP and ODP reports. Luba Jansa and Wolfgang Kuhnt generously shared their personal observations of several cores. Data for the Swiss Pre-Alps project was published by Andre Strasser and colleagues and is from theses at Fribourg University under the direction of Michel Caron. M. Caron and A. Strasser shared their original observations and understanding of the graphic interpretations of these sections. The biostratigraphic data of the Austrian sections were shared by Michael Wagreich, and Stephanie Neuhuber, University of Vienna, made useful suggestions based on her geochemical studies. Diethard Sanders, University of Innsbruck, generously guided me to the Tiefenbach section and shared his data, references, and ideas about this section.

Data for other sections in Appendix 3 were provided by M. Bubík, Czech Geological Survey, Brno; A. Govindan, Asian Biostratigraphic Services, Chennai, India; E. Malata, Jagiellonian University, Krakow; M. Melinte, National Institute of Marine Geology and Geoecology, Bucharest; E.A. Shcherbinina, Geological Institute, Russian Academy of Sciences, Moscow; P. Skupien, VSB–Technical University, Ostrava-Poruba; L. Švábenická, Czech Geological Survey, Prague; and M. Svobodová, Institute of Geology of the Academy of Sciences of the Czech Republic, Prague. H. willems, Bremen University, is curator of biostratigraphic data in three Tibetan sections documented by Weidich for his dissertation; the raw data is not published here but was used to calibrate ages. This paper benefited from the thoughtful comments and suggestions of Paul Sikora, the University of Utah, and Felix Gradstein, University of Oslo.

REFERENCES

Bak, K., 2000, Biostratigraphy of deep-water agglutinated Foraminifera in Scaglia Rossa–type deposits of the Pieneny Klippen Belt, Carpathians, Poland, *in* Hart, M.B., Kaminski, M.A., and Smart, C.W., eds., Proceedings of the Fifth International Workshop on Agglutinated Foraminifera: Grzybowski Foundation, Special Publication 7, p. 15–41.

Bown, P.R., Rutledge, D.C., and Crux, J.A., 1998, Lower Cretaceous, *in* Bown, P.R., ed., Calcareous Nannofossil Biostratigraphy: London, Chapman & Hall, p. 86–130.

Bralower, T.J., Leckie, R.M., Sliter, W.V., and Thierstein, H.R., 1995, An integrated Cretaceous microfossil biostratigraphy, *in* Berggren, W.A., Kent, D.V., Aubry, M.-P., and Hardenbol, J., eds., Geochronology, Time Scales and Global Stratigraphic Correlation: SEPM, Special Publication 54, p. 65–79.

Burnett, J.A., 1998, Upper Cretaceous, *in* Bown, P.R., ed., Calcareous Nannofossil Biostratigraphy: London, Chapman & Hall, p. 132–199.

Carney, J.L., and Pierce, R.W., 1995, Graphic correlation and composite standard databases as tools for the exploration biostratigrapher, *in* Mann, K.O., and Lane, H.R., eds., Graphic Correlation: SEPM, Special Publication 53, p. 23–43.

de Graciansky, P.C. de, Brosse, E., Deroo, G. Herbin, J.-P., Montadert, L., Müller, C., Sigal, J., and Schaaf, A., 1987, Organic-rich sediments and palaeoenvironmental reconstructions of the Cretaceous North Atlantic, *in* Brooks, J., and Fleet, A.J., eds., Marine Petroleum Source Rocks: Geological Society of London, Special Publication 26, p. 317–344.

Enos, P., 1991, Sedimentary parameters for computer modeling, *in* Franseen, E.V., Watney, W.L., Kendall, C.G. St. C., and Ross, W., eds., Sedimentary Modeling: Computer Simulations and Methods for Improved Parameter Definition: Kansas Geological Survey, Bulletin 233, p. 63-100.

Faupl, P., and Wagreich, M., 1992, Cretaceous flysch and pelagic sequences of the Eastern Alps: Correlations, heavy minerals, and palaeogeographic implications: Cretaceous Research, v. 13, p. 387–403.

Fenner, J., 2001, Middle and Late Albian geography, oceanography, and climate and the setting of the Kirchrode I and II borehole sites: Palaeogeography, Palaeoclimatology, Palaeoecology, v. 174, p. 33–65.

Friedrich, O., and Erbacher, J., 2006, Benthic foraminiferal assemblages from Demarara Rise (ODP Leg 207, western tropical Atlantic): possible evidence for a progressive opening of the Equatorial Atlantic Gateway: Cretaceous Research, v. 27, p. 377–397.

Geroch, S., and Nowak, W., 1983, Proposal of zonation for the Late Tithonian–Late Eocene, based upon arenaceous foraminifera from the Outer Carpathians, Poland: Benthos '83, Second International Symposium of Benthic Foraminifera (Pau, April, 1983), p. 225–239.

Gradstein, F., Cooper, R.A., and Sadler, P.M., 2004a, Biostratigraphy: Time scale from graphic and quantitative methods, *in* Gradstein, F., Ogg, J., and Smith, A., eds., A Geologic Time Scale 2004: Cambridge, U.K., Cambridge University Press, p. 49–54.

Gradstein, F., Ogg, J., and Smith, A., 2004b, A Geologic Time Scale 2004: Cambridge, U.K., Cambridge University Press, 589 p.

Guillaume, M., 1986, Révision stratigraphique des couches rouges de la nappe de préalpes médians Romandes: Institute de Géologie, Université de Fribourg, Ph.D. Thése no. 910, 154 p.

Hable, R., 1997, Biostratigraphie, Sedimentologie und Paläogeographische Entwicklung der Préalps Médians de Chablis (Haute Savoie) vom Apt bis Unter-Eozän: Institut für Geologie und Paläontologie, Universität Freiburg, Ph.D. Dissertation No. 1166, 324 p.

Hardenbol, J., and Robaszynski, F., 1998, Introduction to the Upper Cretaceous, *in* de Graciansky, P.-C., Hardenbol, J., Jacquin, T., and Vail, P.R., eds., Mesozoic and Cenozoic Sequence Stratigraphy of European Basins: SEPM, Special Publication 54, p. 329–332.

Harland, W.B., Armstrong, R.L., Cox, A.V., Craig, L.E., Smith, A.G., and Smith, D.G., 1990, A Geologic Time Scale 1989: Cambridge, U.K., Cambridge University Press, 263 p.

Hofman, P., Wagner, T., and Beckmann, B., 2003, Millennial- to centennial-scale record of African climate variability and organic carbon accu-

mulation in the Coniacian–Santonian eastern tropical Atlantic (Ocean Drilling Program Site 959, off Ivory Coast and Ghana): Geology, v. 31, p. 135–138.

Hood, K.C., 1995, Evaluating the use of average composite sections and derived correlations in the graphic correlation technique, *in* Mann, K.O., and Lane, H.R., eds., Graphic Correlation: SEPM, Special Publication 53, p. 83–93.

Houghton, R.L., Thomas, J.E., Jr., and Diecchio, R.J., 1979, Radiometric ages of basalts from DSDP Leg 43: Sites 382 and 385 (New England seamounts), 384 (J-Anomaly), 386 and 387 (Central and western Bermuda Rise), *in* Tucholke, B.E., et al., eds., Initial Reports, DSDP Leg 43: Washington, D.C., U.S. Government Printing Office, p. 739–753.

Hu, X., Jansa, L., Wang, C., and Sarti, M., 2005a, Mid-Cretaceous oceanic red beds in the Umbria–Marche Basin, central Italy: Constraints on paleoceanography and paleoclimate: Cretaceous Research, v. 26, p. 163–186.

Hu, X., Jansa, L., Wang, C., Sarti, M., Bak, K., Wagriech, M., Michalik, J., and Soták, J., 2005b, Upper Cretaceous oceanic red beds (CORBs) in the Tethys: occurrences, lithofacies, age, and environment: Cretaceous Research, v. 26, p. 3–20.

Huff, W.D., 1987, Cretaceous clay mineralogy of the continental rise off the east coast of the United States, Site 603, Deep Sea Drilling Project Leg 93, *in* van Hinte, J.E., et al., eds., Initial Reports of the Deep Sea Drilling Project, v. 93: Washington, D.C., U.S. Government Printing Office, p. 985–988.

Klaver, G.T., van Kempen, T.M.G., Bianchi, F.R., and van der Gaast, S.J., 1987, Green spherules as indicators of the Cretaceous/Tertiary boundary in deep sea drilling project hole 603B, *in* van Hinte, J.E. et al., eds., Initial Reports, DSDP Leg 93: Washington, D.C., U.S. Government Printing Office, p. 1039–1048.

Kuhnt, W., 1990, Agglutinated foraminifera of western Mediterranean Upper Cretaceous pelagic limestones (Umbrian Apennines, Italy, and Betic Cordillera, Southern Spain): Micropaleontology, v. 36, p. 297–330.

Kuhnt, W., Moullade, M., and Kaminski, M.A., 1996, Cretaceous palaeoceanographic events and abyssal agglutinated foraminifera, *in* Moguilevsky, A., and Whatley, R., eds., Microfossils and Oceanic Environments: Aberystwyth, U.K., University of Wales, Aberystwyth Press, p. 63–75.

Miller, F.X., 1977, The graphic correlation method in biostratigraphy, *in* Kauffman, E.G., and Hazel, J.E., eds., Concepts and Methods of Biostratigraphy: Stroudsburg, PA, Dowden, Hutchinson & Ross, Inc., p. 165–186.

Morgiel, J., and Olszewska, B., 1981, Biostratigraphy of the Polish External Carpathians based on agglutinated foraminifera: Microplaeontology, v. 27, p. 1–30.

Moullade, M., Kuhnt, W., and Thurow, J., 1988, Agglutinated benthic foraminifers from Upper Cretaceous variegated clays of the North Atlantic Ocean (DSDP Leg 93 and ODP Leg 103), *in* Boillot, G., Winterer, E.L., et al., eds., Proceedings of the Ocean Drilling Program, Scientific Results, v. 103, p. 349–362.

Neagu, T., 1990, *Gerochammina* n.g. and related genera from the Upper Cretaceous flysch-type benthic foraminiferal fauna, Eastern Carpathians–Romania, *in* Hemleben, C., Kaminski, M.A., Kuhnt, W., and Scott, D.B., eds., Paleoecology, Biostratigraphy, Paleoceanography and Taxonomy of Agglutinated Foraminifera: NATO ASI Series, Kluwer Academic Publishers, v. 327, p. 245–250.

Neuhuber, S., Wagreich, M., Wendler, I., and Spötl, C., 2007, Turonian oceanic red beds in the Eastern Alps: Concepts for paleoceanographic changes in the Mediterranean Tethys from mineralogy, carbonate geochemistry, and stable isotope stratigraphy: Palaeogeography, Palaeoclimatology, Palaeoecology, v. 251, p. 222–238.

Oboh-Ikuenobe, F.E., Benson, D.G., Scott, R.W., Holbrook, J.M., Evetts, M.J., and Erbacher, J., 2007, Re-evaluation of the Albian–Cenomanian boundary in the U.S. Western Interior based on dinoflagellate cysts: Review of Palaeobotany and Palynology, v. 144, p. 77–97.

Obradovich, J.D., Matsumoto, T., Nishida, T., and Inoue, Y., 2002, Integrated biostratigraphic and radiometric study on the Lower Cenomanian (Cretaceous) of Hokkaido, Japan: Proceedings of the Japan Academy, v. 78, ser. B, p. 149–153.

Odin, G.S., and Lamaurelle, M.A., 2001a, The Campanian–Maastrichtian stage boundary, *in* Odin, G.S., ed., The Campanian–Maastrichtian Stage Boundary: IUGS Special Publication (monograph) Series 36, Amsterdam, Elsevier Science B.V., p. 60–67.

Odin, G.S., and Lamaurelle, M.A., 2001b, The Campanian–Maastrichtian stage boundary: Episodes, v. 24, p. 229–238.

Ogg, J.G., Agterberg, F.P., and Gradstein, F.M., 2004, The Cretaceous Period, *in* Gradstein, F.M., Ogg, J.G., and Smith, A.G., eds., A Geologic Time Scale 2004: Cambridge, U.K., Cambridge University Press, p. 344–383.

Premoli Silva, I., and Sliter, W.V., 2002, Practical Manual of Cretaceous Planktonic Foraminifera: University of Perugia, Italy, Dipartimento di Scienze della Terra, 462 p.

Robaszynski, F., Caron, M., Dupuis, C., Amedro, F., Gonzalez Donoso, J.-M., Linares, D., Hardenbol, J., Gartner, S., Calandra, F., and Deloffre, R., 1990, A tentative integrated stratigraphy in the Turonian of central Tunisia: Formations, zones and sequential stratigraphy in the Kalaat Senan area: Centres Recherches Exploration Production Elf-Aquitaine, Bulletin, v. 14, p. 213–384.

Robaszynski, F., Caron, M., Amédro, F., Dupuis, C., Hardenbol, J., Gonzalez Donoso, J.M., Linares, D., and Gartner, S., 1993, Le Cénomanien de la région de Kalaat Senan (Tunisie centrale): Litho-biostratigraphie et interprétation séquentielle: Revue de Paléobiologie, v. 12, p. 351–505.

Sageman, B.B., Rich, J., Arthur, M.A., Dean, W.E., Savrda, C.E., and Bralower, T.J., 1998, Multiple Milankovitch cycles in the Bridge Creek Limestone (Cenomanian–Turonian), Western Interior basin, *in* Dean, W.A., and Arthur, M.A., eds., Stratigraphy and Paleoenvironments of the Cretaceous Western Interior Seaway, USA: SEPM, Concepts in Sedimentology and Paleontology, no. 6, p. 153–171.

Scott, R.W., and Kerans, C., 2004, Late Albian carbonate platform chronostratigraphy, Devils River Formation cycles, west Texas: Courier Forschungs-Institut Senckenberg, v. 247, p. 129–148.

Scott, R.W., Franks, P.C., Evetts, M.J., Bergen, J.A., and Stein, J.A., 1998, Timing of Mid-Cretaceous relative sea level changes in the Western Interior: Amoco No. 1 Bounds Core, *in* Dean, W.A., and Arthur, M.A., eds., Stratigraphy and Paleoenvironments of the Cretaceous Western Interior Seaway, USA: SEPM, Concepts in Sedimentology and Paleontology, no. 6, p. 11–34.

Scott, R.W., Schlager, W., Fouke, B., and Nederbragt, S.A., 2000, Are Mid-Cretaceous eustatic events recorded in Middle East carbonate platforms?, *in* Alsharhan, A.S., and Scott, R.W., eds., Middle East Models of Jurassic/Cretaceous Carbonate Systems: SEPM, Special Publication 69, p. 77–88.

Scholle, P.A., Arthur, M.A., and Ekdale, A.A., 1983, Pelagic environment, *in* Scholle, P.A., Bebout, D.G., and Moore, C.H., eds., Carbonate Depositional Environments: American Association of Petroleum Geologists, Memoir 33, p. 619–691.

Shaw, A.B., 1964, Time in Stratigraphy: New York, McGraw-Hill, 365 p.

Strasser, A., Caron, M., and Gjermeni, M., 2001, The Aptian, Albian and Cenomanian of Roter Sattel, Romandes Prealps, Switzerland: a high-resolution record of oceanographic changes: Cretaceous Research, v. 22, p. 173–199.

Wagreich, M., 2002, Cretaceous oceanic red beds in Austria Alps, *in* Hu, X., and Sarti, M., eds., IGCP Project 463, Cretaceous Oceanic Red Beds (CORB) in an Apennines–Alps–Carpathians Transect: University of Ancona, Italy, Institute of Marine Sciences, Field Guidebook, September, 2002, p. 30–46.

Wagriech, M., 2006, Overview of CORBs in the Eastern Alps (Austria) (abstract), *in* Hu, X., Wang, Y., and Huang, Y., eds., International

Symposium on Cretaceous Major Geological Events and Earth System—Workshop on Cretaceous Oceanic Red Beds (IGCP 463 & 494): China University of Geosciences, Beijing, China, p. 89–90.

WAGREICH, M., AND KRENMAYR, H.-G., 2005, Upper Cretaceous oceanic red beds (CORB) in the Northern Calcareous Alps (Nierental Formation, Austria): slope topography and clastic input as primary controlling factors: Cretaceous Research, v. 26, p. 57–64.

WAGREICH, M., AND NEUHUBER, S., 2005, Stratigraphy and geochemistry of an Early Campanian deepening succession (Bibereck Formation, Gosau Group, Austria): Earth Science Frontiers (China University of Geosciences, Beijing, Peking University), v. 12, p. 123–131.

WOOD, C.J., ERNST, G., AND RASEMANN, G., 1984, The Turonian–Coniacian stage boundary in Lower Saxony (Germany) and adjacent areas: the Salzgitter–Salder Quarry as a proposed international standard section: Geological Society of Denmark, Bulletin, v. 33, p. 225–238.

APPENDICES

APPENDIX 1.—Section Catalog Files for projects MIDK3.cat, MIDK4.cat, MIDK41.cat, MIDK42.cat. List of global reference sections that define the Cretaceous graphic correlation database and CORB sections in the graphic correlation experiment. The MIDK42CS database was compiled in four stages: I) MIDK3, II) MIDK4, III) MIDK41, and IV) MIDK42. Section files of outcrops and boreholes on CD or University of Tulsa Geosciences website.

Part I. The following sections comprise the MIDK3 1994-1995 database: Catalog File: C:\GRAPHCOR\MIDK3.CAT, Date modified 12/03/2001.

Section File	Section Name
MIDK.1	Kalaat Senan, Turonian Reference section of Coniacian
MIDK.2	Harland Geologic Time Scale, 1990: Standard Reference Section
MIDK.3B	Santa Rosa Canyon Section, Mexico
MIDK.4	DSDP 547, Offshore Morocco
MIDK.5	DSDP 545, Offshore Morocco
MIDK.6	Type Cenomanian section, France
MIDK.7	Djebel Bireno, Tunisia,
MIDK.8	Djebel Mrhila, Tunisia,
MIDK.9	Amoco No. 1 Bounds core, Kansas
MIDK.10	Kalaat Senan, Tunisia Section
MIDK.11	DSDP 386 Bermuda Plateau, Atlantic
MIDK.12	Boulonnaise Section, France
MIDK.13	Piobbico Core, Marche, Italy
MIDK.14	DSDP 369A, Offshore Morocco
MIDK.15	Pueblo, Colorado outcrop
MIDK.16	Wadi Miaidin, Oman, Scott, '90,
MIDK.17	Wadi Miaidin, Oman, Simmons, '87
MIDK.18	Shell No. 1 Chapman Core, Texas
MIDK.19	Shell No. 1 Tomasek Core, Texas
MIDK.20	Trinity River, Texas Section
MIDK.21	Austin, Texas Composite Section
MIDK.22	Nahr Ibrahim, Lebanon
MIDK.23	Dlebta-Chenin Aair, Lebanon
MIDK.24	Mt. Risou, Rosans, SE France, Cenomanian GSSP
MIDK.25	Cap Blanc-Nez Revised, France
MIDK.26	Cismon Section, Italy (VU Data)
MIDK.27	Pie' del Dosso Section, Italy
MIDK.28	Estella Basin, NW Spain
MIDK.29	Eastbourne, UK
MIDK.30	Selbukhra Section, Crimea
MIDK.31	Kef el Azreg, Tunisia
MIDK.32	Sopeira Section, Pyrenees,
MIDK.33	Flamicell Section, Pyrenees
MIDK.34	Montsec Section, Pyrenees
MIDK.35	Peace River Composite, Canada
MIDK.36	Anderson Husky Roros, Canada
MIDK.37	Type Shell Creek Fm., Wyoming
MIDK.38	Ida ou Tanane, Morocco
MIDK.39	Chichaoua I, Morocco
MIDK.40	Timinoun, Morocco
MIDK.41	ODP 641C, Offshore Portugal
MIDK.42	42-Cassis, France C-T Reference
MIDK.43	43-Gorgo a Cerbara Section, Italy, Potential Aptian GSSP
MIDK.44	44-Culver Cliff, SE England
MIDK.45	45-Mobil Core 16, Dallas, TX
MIDK.46	46-North Colo Front Range
MIDK.47	47-Wadi Miaidin, Oman, Philip
MIDK.48	48-Blanc-Nez Composite, France
MIDK.49	49-Smedmore-Blackgang, Isle of Wight, UK
MIDK.51	Grayson Bluff, Denton Co., TX
MIDK.55	Monte Petrano, Central Italy, Proposed Albian GSSP

APPENDIX 1. (continued).

Part II. The following sections comprise the MIDK4 database: Catalog File: C:\GRAPHCOR\MIDK4.CAT, Date = 01/15/2001; modified 05/21/02, 09/09/02

Section File	Section Name
MIDK3CS.1	MIDK3 CS: Standard Reference Section
MIDK.16B	16B Wadi Miaidin, Oman (Scott, 1990)
MIDK.26B	26B Cismon Core, Italy
MIDK.400	400 Wadi Bani Kharus, Oman
MIDK.403	403 Gorbea section, Northern Spain
MIDK.406	406 Wadi El Assyi, Oman
MIDK.50	50 Wadi Miadin Section Seq Strat
MIDK.51	51 Grayson Bluff, TX
MIDK.52	52 Aube France, Lower-Mid Albian
MIDK.53	53 Weald Anticline, England, Apt-Alb
MIDK.54	54 Folkestone, England, Mid-Upper Alb
MIDK.60	60 Estella-Lizarra section, N. Spain
MIDK.61	61 Dukhan-B, Qatar
MIDK.66	66 Jebel Areif El Naqa, Sinai, Egypt
MIDK.67	67 Gebel Abu Zurub, Sinai, Egypt
MIDK.68	68 Gebel Guna, Sinai, Egypt
MIDK.69	69 Coupe de la Gare de Cassis, SE France
MIDK.71	71 Guerrero-Morelos Basin, S. Mexico
MIDK.72	72 Oued Melleque, Tunisia
MIDK.73	73 Cres Island, Croatia section
MIDK.74	74 Antruiles, Trento Plateau, Italy
MIDK.75	75 North Huqf, Oman, section S 001
MIDK.76	76 North Huqf, Oman, section S 008
MIDK.77	77 North Huqf, Oman, section D 005
MIDK.78	78 Oued Bahloul, central Tunisia
MIDK.79	79 Kef Hahouner, Algeria
MIDK.80	80 Sierra del Carche Prebetic zone, Spain
MIDK.81	81 Dugi Otok, Croatia
MIDK.84	84 DSDP Core Hole 549, SW Offshore England
MIDK.88	88 Chimana Grande, Venezuela
MIDK.89	89 Stanolind #1 Schmidt, Guadalupe Co., Texas
MIDK.90	90 Lower Mondego River, Northern Portugal
MIDK.91	91 Composite Carbonate Section, Southern Portugal
MIDK.92	92 Composite Section, Portugal
WOODCS.1	Tur-Con Comp. Std. Section, N. Germany
PECOSCS.1	Pecos River Comp. Std. Section, TX
MIDKPAL.35	ODP 1050C Blake Nose, W. Atlantic
Tibetk.1	Tibetk 1 Zongshan Section
Tibetk.2	Tibetk 2 Willems' Tingri Section
Tibetk.3	Tibetk 3 Hu's Tingri Section
Tibetk.4	Tibetk 4 Willems' Gamba section A1
Tibetk.5	Tibetk 5 Willems' Gamba section A2
Tibetk.6	Tibetk 6 Willems' Gamba section B
Tibetk.7	Tibetk 7 Chuangde Section, Guangze
Tibetk.8	Tibetk 8 Gongzha Section, Tingri, Tibet
UPK.1	UPK 1 Austin Gp., Austin, TX
UPK.2	UPK 2 Austin Gp., Dallas, TX
UPK.3	UPK 3 Olazagutia, Spain
UPK.4	UPK 4 Zumaya, Spain
UPK.5	UPK 5 El Kef K/T boundary
UPK.6	UPK 6 Hendaye, Spain
UPK.7	UPK 7 Bidart, Spain
UPK.8	UPK 8 Sopelana, Spain
UPK.11	UPK 11 Gosau Valley Composite, Austria
UPK.12	UPK 12 Tercis Quarry section, France (Kennedy)
UPK.13	UPK 13 Tercis Quarry section, France (Odin)
UPK.14	UPK 14 Lepsa, E. Carpathians, Romania
UPK.15	UPK 15 Flamicell-Pallaresa, Pyrennes, Spain
PAL.111	PAL 111 ODP 758 NE Indian Ocean
PAL.121	121 ODP 762C Exmouth Plateau, Indian Ocean
PAL.131	131 DSDP 515F Western Atlantic
PAL.141	PAL 141 ODP 752 Indian Ocean
PAL.151	PAL 151 DSDP 550+550B NE Atlantic
PAL.161	PAL 161 DSDP 548A NE Atlantic
PAL.211	PAL 211 ODP 690B Weddell Sea, Antarctica
BAPTCS.1	Base Aptian Ammonite Composite Section
MURAL.1	Lampazos, Sonora Section
MURALCS.1	Mural Composite of Sonora Sections

APPENDIX 1. (continued).

Part III. The following sections comprise the MIDK41 database: Catalog File: C:\GRAPHCOR\MIDK41.CAT, Dat e= 11/21/2004.

Section File	Section Name
NEWKAGES.1	2004 Ages Modified (Gradstein et al., 2004): Standard Reference Section
MIDK4CS.1	Composited data of MIDK4.cat 11-18-04
MIDK.9B	Bounds, Core, Kansas – Niobrara Fm. only
MIDK.11B	11B DSDP 386 Upper & Lower Cretaceous
MIDK.15	15 Pueblo Colorado – Niobrara Fm. only
MIDK.15B	15B Pueblo, Colorado, Turonian GSSP
MIDK.20B	20B Trinity River Composited Section Revised
MIDK.21B	21B Colorado River Composited Section Revised
MIDK.57	57 Tartonne, France, Aptian-Albian
MIDK.58	58 Pre-Guitard, France, Aptian-Albian
MIDK.85	85 Blanco River, TX Composited Section
MIDK.86	86 Leon River, Tx Composited Section
MIDK.93	93 Gulf McAlpin Well, Louisiana
MIDK.95	95 Shell 4898 # 1, Chandeleur Sound, Louisiana
MIDK.96	96 Shell 4898 # 2, Chandeleur Sound, Louisiana
MIDK.97	97 Ballard Carey-Carolla No. 1, Texas
MIDK.98	98 Roter Sattel, Switzerland
MIDK.99	99 Zasan Section, Poland
MIDK.100	100 Cassis, France Cenomanian-Turonian
MIDK.101	101 Font-Blanc, France Cenomanian-Turonian
UPK.10	UPK 10 Tiefenbach, Brandenburg, Austria
UPK.17	UPK 17 Casamance Well 10, Offshore W. Africa – Kuhnt Data
UPK.18	UPK 18 Bottacione Gorge, Italy – Khunt Data
UPK.19	UPK 19 Red Bird Section, Wyoming
UPK.21	UPK 21 Forwark Quarry, Poland
UPK.22	UPK 22 Hacho de Montejaque, Spain
CORB382.1	DSDP 382 Central Atlantic
CORB385.1	DSDP 385 Central Atlantic
CORB398D.1	DSDP 398D, Eastern Atlantic
CORB603B.1	DSDP 603B Western Atlantic
CORB641A.1	ODP 641A North Central Atlantic
CORBCOVA.1	Covasna Valley, Siclau, Romania
CORBPOL.14	14 Zasadne Section, Poland
CORBBYST.1	Bystry Creek Section, Czech Republic v
CORBRUS.1	Khalagork, Caucasus, Russia (corbrus-1) Tur
CORBROM.1	Pietrosita, Romania (corbrom-1) – Melinte
CORB.25	25 Plagersflue, Switzerland (corb-25) - Caron
CORB.26	26 Ouzon, Switzerland (corb-26) - Caron
CORB.27	27 Buchberg, Austria – Wachreich
CORB.28	28 Oberschau, Austria – same
CORB.29	29 Oberhehenfeld, Austria – same
CORB.30	30 Hofergraben, Austria – same
CORB.31	31 Lattengebirge, Austria – same
CORB.32	32 Rehkogel RED, Austria – same
CORB.33	33 Rehkogel CT, Austria – same
CORB.34	34 Postalm-Retschegg, Austria - same

APPENDIX 1. (continued).

Part IV. The following sections comprise the MIDK42 database: Catalog File: C:\GRAPHCOR\MIDK42.CAT, Date = 08/15/2006. MIDK4.cat was modified by graphing sections spanning Cenomanian–Turonian boundary to MIDK41CS.1 to re-calibrate revised age of Cenomanian–Turonian boundary.

Section File	Section Name
MIDK41CS.1	MIDK41 CS
MIDK.16B	16B Wadi Miaidin, Oman (Scott, 1990)
MIDK.60	60 Estella-Lizarra section, N. Spain
MIDK.66	66 Jebel Areif El Naqa, Sinai, Egypt
MIDK.67	67 Gebel Abu Zurub, Sinai, Egypt
MIDK.68	68 Gebel Guna, Sinai, Egypt
MIDK.71	71 Guerrero-Morelos Basin, S. Mexico
MIDK.72	72 Oued Melleque, Tunisia
MIDK.74	74 Antruiles, Trento Plateau, Italy
MIDK.78	78 Oued Bahloul, central Tunisia
MIDK.81	81 Dugi Otok, Croatia
MIDK.84	84 DSDP Core Hole 549, SW Offshore England
MIDK.88	88 Chimana Grande, Venezuela
MIDK.90	90 Lower Mondego River, Northern Portugal
MIDK.91	91 Composite Carbonate Section, Southern Portugal
MIDK.92	92 Composite Section, Portugal
MIDKPAL.35	ODP 1050C Blake Nose, W. Atlantic
Tibetk.1	Tibetk 1 Zongshan Section
Tibetk.2	Tibetk 2 Willems' Tingri Section
Tibetk.3	Tibetk 3 Hu's Tingri Section
Tibetk.4	Tibetk 4 Willems' Gamba section A1
Tibetk.5	Tibetk 5 Willems' Gamba section A2
Tibetk.6	Tibetk 6 Willems' Gamba section B
Tibetk.7	Tibetk 7 Chuangde Section, Guangze
UPK.15	UPK 15 Flamicell-Pallaresa, Pyrennes, Spain
PAL.121	121 ODP 762C Exmouth Plateau, Indian Ocean

APPENDIX 2.—Cretaceous stage type localities, criteria, and GSSPs in MIDK42 database. Comparison of three time scales: MIDK42, August 2006, Hardenbol et al. (1998), and Gradstein et al. (2004, fig. 19.1) (boundary criteria from Gradstein et al. 2004). Some datums not reported (NR).

	MIDK42	1998	2004
K/T Boundary: K/T Iridium Anomaly	**65.55 Ma**	**65.0**	**65.5**
Base MAASTRICHTIAN	**72.60**	**71.3**	**70.6**
GSSP – Tercis les Bains, SW France (UPK.13);			
Criterion – mean of 10 horizons at 90 cm			
Below FO of *Pachydiscus neubergicus*	> 72.58	> 71.29	> 70.6
And FO *Hoploscaphites constrictus*	72.22	NR	NR
FO *Gansserina gansseri*	75.33	72.84	72.0
FO *Baculites jenseni*	72.38	72.10	71.56
Mid Chron C32n.2n	73.49–71.87	72.5	72.5
FO *Belemnella obtusa*	NR	70.66	70.5
LO *Quadrum trifidum*	68.08	70.97	69.9
Near base of Chron C31r	70.46	70.97	~70.5
LO *Radotruncana calcarata*	74.2	75.21	NR
Base CAMPANIAN	**83.70**	**83.5**	**83.5**
No GSSP – Aubeterre-sur-Dronne, France; England; Texas			
FO *Placenticeras bidorsatum* (in UPK.11)	83.68	83.5	~83.5
LO *Marsupites testudinarius*	NR	NR	~83.5
Near base Chron C33r	83.37	< 83.50	~83.5
Top C34n	83.37	83.50	84.0
FO *Desmoscaphites bassleri*	NR	84.05	83.9
Base SANTONIAN	**85.91**	**85.8**	**85.8**
Saintes, France; candidate GSSP Olazagutia, Spain (UPK.3)			
FO *Cladoceramus undulatoplicatus*	85.91	85.79	~85.8
In Chron C34n	> 83.37	> 83.50	NR
Base CONIACIAN	**88.52**	**89.00**	**89.3**
Richemonte Seminary, Cognac, France; Forwark Quarry, Poland, UPK.21)			
Candidate GSSP at Salzgitter/Salder quarry, Germany (Woodcs.1)			
FO *Cremnoceramus deformis erectus*	88.41	NR	~89.3
(= *C. rotundatus* of Tröger)	88.52	88.96	
FO *Forresteria petrocoriensis* [sp. in MIDK42]	88.50	88.96	89.07
Base TURONIAN	**93.00**	**93.5**	**93.5**
GSSP – Rock Canyon Anticline, Pueblo, Colorado (MIDK.15b)			
Correlated with bentonites dated at 93.25 ± 0.55 Ma and 93.55 ± 0.4 Ma			
FO *Watinoceras devonense*	92.95	93.49	93.55
In OAE2	93.55–92.86	NR	NR
Base CENOMANIAN	**97.13**	**98.9**	**99.6**
GSSP – Mont Risou, SE France (MIDK.24)			
FO *Rotalipora globotruncanoides*	97.13	99.15	99.6
FO *Rotalipora brotzeni*	97.08	NR	NR
Below FO *Mantelliceras mantelli*	97.07	98.9	99.6
Base ALBIAN	**112.75**	**112.2**	**112.0**
Aube region, France (MIDK.57)			
Previous criteria:			
FO *Leymeriella tardefurcata*	112.74	112.2	112
FO *L. schrammeni*	NR	112.2	NR
FO *Farnhamia farnhamensis*	113.11	111.65	NR
Base Black Shale Markers Jacobi bed	122.10	NR	NR
FO *Prediscosphaera columnata*	122.85	110.06	112.0
Base Killian bed	116.53	NR	NR
LO *Hypacanthoplites jacobi*	112.93	112.2	113.2
Base Paquier bed	112.72	NR	NR
FO *Douvielliceras* ex. gp. *mammillatum*	112.27	110.06	110.8
Base APTIAN	**124.60**	**121.0**	**125.0**
Candidate GSSP Gorgo a Cerbara, Italy; Apt, France (MIDK.43, MIDK.69)			
FO *Deshayesites oglanlensis/tuarkyricus*	124.55	120.98	122.9
FO *Prodeshayesites* spp. (*D. obsoletus*)	124.89	120.49	NR
Base Chron CM0r	125.00	120.98	125.0
Base OAE1a	123.05	NR	NR
Base Selli level	123.06	NR	NR
Base BARREMIAN	**130.23**	**127.0**	**130.0**
Candidate GSSP Rio Argos, Spain; Gorgo a Cebara, Italy (MIDK.43)			
FO *"Spitidiscus" hugii*	NR	127.03	130.0
FO *Avramidiscus [Spitidiscus] vandeckii*	130.23	NR	128.3
Upper part Magnetochron CM5r	130.78	NR	NR

APPENDIX 3.—Cretaceous integrated ranges in MIDK42 database.

STAGES/CHRONS	AMMONITES FOs	PLANKTIC FORAMS FOs	CALCAREOUS NANNOPLANKTON	DINOFLAGELLATES	BENTHIC FORAMS
					LO C. gigantea 65.40
C29r 64.74					LO S. praelonga 65.40
					LO S. placenta 65.40
MAASTRICHTIAN 65.5		LO G. gansseri 65.57	LO L. grilli 65.95		LO R. epigona 65.56
Iridium – 65.55 Ma		LO A. mayaroensis 65.75	LO P. asper 66.13		LO C. crassa 66.36
C30n 65.89	A. terminus 66.96		FO M. prinsii 66.75		LO M. varians 66.36
C30r 67.59			LO E. eximius 67.69		
C31n 67.70			FO M. murus 68.17		
C31r 68.22			LO U. trifidus 68.21		
			LO R. levis 68.38		
			FO L. quadratus 68.77		
			FO N. frequens 69.17		
		A. mayaroensis 69.46	LO T. orionatus 69.17		
C32n 70.46	A. fresvillensis 70.33	R. fructicosa 70.08	LO P. constricta 69.56		
	P. neubergericus 72.58			LO P. truncigerum 72.48	
CAMPANIAN 72.6		G. (C.) contusa 72.84			
C32r 73.49		G. gansseri 73.95		LO P. infusorioides 73.31	
C33n 73.93	N. hyatti 74.56	LO R. calcarata 74.16			FO R. epigona 74.44
	D. cheyennense 74.61	G. aegyptiaca 74.20	FO M. pleniporus 74.99		
		R. [G.] calcarata 75.56		LO O. costata 75.63	
	B. polyplocum 76.05		FO U. trifidus 76.19	LO O. operculata 76.30	FO S. praelonga 76.02
			FO U. sissinghii 76.74	LO T. castanea 76.30	FO G. rugosa 76.11
			FO U. gothicus 76.98		FO D. crassa 76.66
					LO U. jankoi 77.21
					FO R. inclusa 77.38
C33r 78.59			FO C. aculeus 79.04		
			LO M. furcatus 82.27		FO T. amorpha 81.97
	D. delawarensis 83.15	LO D. asymmetrica 83.21			
C34n 83.37	P. bidorsatum 83.58				
	P. polyopsis 83.63		FO B. parca parca 83.53		
SANTONIAN 83.7		G. ventricosa 84.01	FO R. levis 83.84		FO K. coniformis 84.38
	T. gallicus 85.00	G. elevata 85.03	LO L. septenarius 85.51		FO B. problematicus 85.08
		LO D. primitiva 85.72			
CONIACIAN 85.9					LO U. praejankoi 86.12
		D. asymetrica 86.37			FO C. gigantea 86.36
					LO G. stanislawi 86.86
	P. serratomarginatus 87.83				
			FO L. grillii 88.20		LO P. obtusa 88.22
	Forresteria sp. 88.50		FO A. cymbiformis 88.24		

APPENDIX 3 (continued).

STAGES/CHRONS	AMMONITES FOs	PLANKTIC FORAMS FOs	CALCAREOUS NANNOPLANKTON	DINOFLAGELLATES	BENTHIC FORAMS
TURONIAN 88.50			FO M. decussata 88.52		
		D. concavata 88.65	FO M. furcatus 88.941		
		D. primitiva 89.72	FO K. magnificus 89.60		FO H. excelsa 89.75
			LO C. kennedyi 90.17	FO H. difficile 90.29	
			LO L. septenarius 90.23		
			LO L. acutus 90.36	FO S. protusa 90.44	FO C. crassa 91.39
			LO H. chiastia 90.39	FO e. spinosa 90.47	FO C. ovulum 91.71
			LO A. albianus 90.70		FO U. praejankoi 91.89
			FO E. eximius 90.72	LO C. obliquicostatum 90.77	FO U. jankoi 91.96
	C. woollgari 92.35	M. sigali 92.61			FO S. placenta 92.59
	M. nodosoides 92.72				FO K. grzybowskii 92.73
	W. devonense 92.95	H. helvetica 92.92			FO G. conversa 92.90
					FO G. lenis 92.90
CENOMANIAN 93.00	N. judii 93.13				LO A. preslii 93.01
	C. naviculare 93.41		FO C. biarcus 93.44	FO S. pontis-mariae 93.50	
			FO Q. gartneri 93.55	LO L. siphoniphorum 93.50	
	C. guerangeri 94.0		FO A. octoradiata 93.84		
	A. jukesbrownei 94.6				FO H. bulloides 94.50
	C. inerme 95.3	W. archeocretacea 94.55	FO G. segmentatum 94.84	LO O. verrucosum 94.96	
	A. rhotomagense 95.3	D. algeriana 95.20			
	M. dixoni 95.8	R. reicheli 96.71			
		R. brotzeni 97.08	FO L. acutus 96.17	FO C. membraniphorum 95.94	
		R. greenhornensis 97.08	FO C. kennedyi 96.55	FO E. rugulosum 96.51	LO R. minuta 96.20
	M. mantelli 97.07	R. globotruncanoides 97.13			
ALBIAN 97.13			FO C. anfractus 97.17		
	S. dispar 98.64		LO H. albiensis 97.37	FO E. spinosa 97.80	FO P. irregularis 97.54
			FO G. nanum 98.30	FO A. deflandrei 97.82	FO H. kirki 98.09
			FO E. eximius 98.67	FO O. verrucosum 98.80	
		R. appenninica 100.37	FO E. turriseiffelii 101.86	FO P. infusorioides 101.26	
	M. inflatum 102.98				FO R. minuta 102.07
				FO C. obliquicostatum 104.16	FO H. concavus 103.30
	D. cristatum 105.54			FO F. clavigera 106.11	
				FO O. costata 106.30	
			FO E. monechiae 107.30		
			FO A. albianus 109.77	FO A. tutulosa 109.06	
				FO L. siphoniphorum 110.12	
				FO X. alatum 112.64	
				FO D. cladoides 112.64	